

First of all, we would like to sincerely acknowledge the referees for their detailed reviews of our manuscript, which will certainly allow us to improve its quality. We have carefully considered all of their comments and suggestions and outlined our responses below, detailing how we have modified the text and figures accordingly.

**Referee 1: Laura Giambiagi**

**Comment:** 1) *Tectonic setting: To give the manuscript a broader impact, I suggest adding a tectonic setting section, which can be integrated into the Geological-tectonic setting, with a synthesis of the Cenozoic extensional and compressional phases, and a description of the main structures of the area. Also, I would add a description of the Miocene intrusive complexes, such as the La Obra batholith.*

**Author's response:** in the new version of the manuscript, the tectonic context is more extensively discussed in the Geological Background section, included an expanded synthesis of the main extensional and compressional phases, and the main fault systems active during these periods. The descriptions of the La Obra batholith and the Carlota intrusive complex were expanded at the Results section.

**Comment:** 2) *Lithospheric-scale structures: Since there is no evidence that these fault systems involve the continental lithosphere, it is more convenient to name them as "continental-scale structural systems" (as they are called in the Discussion section). An alternative approach could be to use the available geophysical data and clearly propose the connection between the crustal structures and deeply-seated anisotropies. These geophysical data/analyses are just mentioned, but not properly presented as a discussion.*

**Author's response:** a new discussion and additional references were added to the text, to explain why we think this fault system is of lithospheric scale: *"Even though the whole lithosphere involvement of these continental-scale structures has not been demonstrated empirically in the Andes, several lines of reasoning provide independent arguments to support this concept. In one hand, Yáñez and Rivera (2019) proposed that the origin of these deep-seated structures could be related with master and transform faults associated with ancient rifting and/or suture zones related to collisional processes. In both likely scenarios, recent analogues show the presence of deep seated structures that involve the whole lithosphere (i.e. Kuna et al., 2019; Hua et al., 2019). On the other hand, several authors have demonstrated that continental-scale deformation zones, of some hundreds of kilometres length (comparable in scale to the PFS/MDZ), are controlled by the rheology of the mantle (i.e. Bird and Piper, 1980, England and McKenzie, 1984). Moreover, numerical models, in agreement with field observations, indicate that deformation decays laterally to 1/10 of the structure length for strike-slip dominated movements (England et al., 1985), thus developing a deformation zone of 10-30 km width, similar to the PFS/MDZ."*

**Comment:** 3) *Kinematic vs dynamic analysis of fault-slip data: This must be more deeply discussed. Why do the authors perform these two kinds of analyses? What are the reduced stress tensors obtained from fault-slip data close to a major long-lived trans-crustal fault system telling us in terms of dynamics? Can they be interpreted as reflecting the stress of the crust during the movement of these structures? Since these structures have been previously generated during at least the Oligocene extension, or probably before (as the authors mention in the Discussion), these*

tensors are not probably reflecting a stress field because, in this case, one of the basic assumptions during the inversion technique, the one concerning the absence of interference between faults, is not properly fulfilled. I suggest that the authors discriminate between stations close to the main faults, from stations located far away from the main faults. For example, data from the Piuquencillo Alto area could be separated into two (close and apart from the NW fault).

**Author's response:** regarding the use of the kinematic and dynamic analyzes, we preferred to do both to be able to compare the results of these two different approaches and, from that, provide a stronger support to our interpretations. A new discussion about the possible perturbations/rotations of the stress tensor in the vicinity of a major fault was added (*"When interpreting the results of stress tensor calculations from the inversion of fault slip data, a possibility which has to be considered is that stress tensor rotations might occur in the vicinity of major faults, although the expected patterns of stress rotation are still a matter of debate (Hardebeck and Michael, 2004; Famin et al., 2014). If these stress tensor rotations occurred at the PFS, then part of our calculations might not represent a regional stress field, but a local stress tensor acting only in and around the fault traces. The dynamic analysis by sector, however, suggests that this is not the case. The Piuquencillo Alto and Piuquencillo-Claro sectors cover areas around the main traces of the PFS, while the Maipo sector is located further away from it (Fig. 13). In these three sectors, the direction of maximum horizontal compression is similar (E-W to slightly ENE), without any evidence of rotations occurring around the traces of the PFS. The results obtained are also consistent with regional calculations of the Miocene – early Pliocene stress field in central Chile (Piquer et al., 2016). All of this is consistent with the fact that none of the cropping-out branches of the PFS is individually a major fault; the strain associated to each of them is of small magnitude, so no major perturbations of the stress tensor are expected around them"*). We followed the suggestion of exploring possible differences in the area of Piuquencillo Alto between structural stations located at or close to the main NW-striking faults, and those located further away. However, the results do not show major differences, in both cases indicating a strike-slip regime with ENE-trending shortening and NNW stretching. Furthermore, no major differences are observed in the orientation of the kinematic axes or the calculated paleo-stress tensor between the Piuquencillo Alto, Piuquencillo-Claro and Maipo sectors, despite the fact that the latter is located further away from the main branches of the PFS. The results obtained are also consistent with regional calculations of the stress tensor during the Miocene – early Pliocene, presented in previous publications (Piquer et al., 2016). All of this is consistent with the fact that none of the cropping-out branches of the PFS is individually a major fault; we interpret that they represent the manifestation at the present-day surface of a major fault in the Andean basement, but the strain associated to each of the individual fault observed in the field is of small magnitude. Therefore, we conclude that there are no major perturbations of the regional stress tensor related to the individual fault traces of the PFS.

**Comment:** 4) *Age of dikes and intrusives: You should clarify the relationship between the emplacement of dikes and intrusives, and movement along the study fault system. Are there any time constraints on this relationship? For example, what is the age of the Ag-Pb-Zn-Cu vein system in the San Pedro de Nolasco sector? In this respect, move paragraph 182-186 from the Discussion section to the Results section, and add any other information about the timing of emplacement of these intrusives and the timing of slips of the studied faults.*

**Author's response:** a more detailed discussion was included about the timing of dikes and veins, and why we can assign them a middle to late Miocene age. However, this can only be done based on cross-cutting relationships and correlations; there are no radiometric ages of the dikes emplaced along the PFS or of the vein system. We only have U-Pb ages of major plutons, and there are previously-published K-Ar and U-Pb ages of volcanic rocks. We attempted to obtain U-Pb zircon ages from the dike swarms, however no zircons were found in any of the collected samples. Regarding the veins, we also attempted to obtain an  $^{40}\text{Ar}/^{39}\text{Ar}$  age from syn-tectonic hydrothermal actinolite in Piuquencillo Alto, however, the calculated ages are not geologically possible; they are several My older than the U-Pb ages of the intrusive unit which hosts the veins. Regarding the paragraph in lines 182-186, this is now included in the Discussion section, following the suggestion of the Topical Editor regarding moving the paleo-stress tensor calculations entirely to the Discussion chapter.

**Comment:** 5) *The fluid pathways: This idea must be broadened. Discuss here how sigma 1 is obtained. Are WNW and ENE conjugated strike-slip faults, or not? For each measurement station, add the main strike of dextral and sinistral faults, as well as the orientation of local stress tensor axes, and then compare them. As I pointed out above, it would be nice to have had previously discrimination between tensors obtained close to or far apart from the main faults. It is not clear to me why the ENE striking faults are optimally-oriented for the migration of fluids, while the WNW striking faults are not. If both sets are conjugate strike-slip faults, as stated in lines 201-202, why is one set more likely to dilate and the other one more likely to slip? In my opinion, more information about the strike of the local sigma 1 is needed to evaluate this proposal. Add a table containing: location of each station, number of measured faults, results of fault-slip inversion (orientation of principal stress axes and stress ratio), and lapse of time for each calculated reduced stress tensor.*

**Author's response:** regarding the first point, as mentioned before, we added a discussion regarding the possible variations in the stress tensor between structural stations located close to or far apart from the main branches of the PFS. A new figure was added showing the strike of faults with a sinistral and dextral component (Fig. 16 in the new version of the manuscript), and a table with all the data from our structural stations is now included as Supplementary material. We added a clearer explanation of why we think ENE-striking faults were more favorably oriented for dilation than NW-striking faults (*"This suggests that the PFS and the ENE-striking faults acted broadly as conjugate faults under the prevailing middle Miocene – early Pliocene stress tensor. However, they are not oriented at the ideal angle with respect to  $\sigma_1$  expected in intact rocks, with the ENE-striking faults being more parallel to  $\sigma_1$  than the fault planes of the PFS. The reason for this might be that both sets of faults are part of large-scale, pre-existing fault systems (the PFS and, for the ENE-striking faults, the Yeso Valley Fault System), reactivated during the Mio-Pliocene, but not originated as conjugate structures. As the ENE-striking faults are more parallel to the predominant orientation of  $\sigma_1$  (E-W to ENE-trending), they were the most favourably oriented for opening, which explains why ENE-striking veins are as common as those striking WNW, while ENE-striking fault planes are much less frequent"*). As explained in the text, we think both sets of faults are part of large-scale, pre-existing fault systems (the PFS and the Yeso Valley faults). These fault systems acted broadly as conjugate faults under the prevailing Mio-Pliocene stress tensor, but they were not originated as such; because of this, they are not oriented at the ideal angle with respect to  $\sigma_1$  expected in intact rocks, and one of the fault sets is more parallel to  $\sigma_1$  than the other.

**Comment:** 6) *Transient stress reversals: This statement is very questionable. It is difficult to explain a change from compression to extension as stress reversals during the coseismic stress release. Positive changes in the Coulomb failure stress (see Harris et al. 1998; Stein, 1999; King and Cocco, 2000; Freed 2005) bring receiver faults in the continental crust closer to failure, but the magnitudes involved in these stress changes are small (<1 MPa). The process is more related to the unclamping of the receiver faults, due to a drop in the normal stress that prevents the slip during the interseismic period. See Spagnotto et al (2015), who explore how changes in the Coulomb conditions associated with the Maule earthquake triggered upper-plate earthquakes. They argue that the reactivation of faults after a mega-earthquake at the subduction interphase derives from unclamping processes associated with co-seismic dilatation deformation inferred from GPS observations.*

**Author's response:** we agree that “stress reversal” is probably not appropriate wording; we changed it to “stress relaxation, leading to transient local extension” in the new version of the manuscript. We added a reference to the very interesting work of Spagnotto et al. (2015). We do not intended to say that an extensional stress regime is established regionally during co-seismic periods. Our point is that, as is also mentioned in the referee's comment, co-seismic dilation cause a drop in the normal stress in faults broadly perpendicular to  $\sigma_1$ , which, particularly under high fluid pressures, can lead to fault activation with normal kinematics (as shown recently by the activation of the Pichilemu fault after the Maule earthquake).

All the corrections included as “minor comments” in the letter were incorporated to the manuscript, with the following exceptions:

**Line 75:** *Here I wonder how are these sheeted dikes related to mineralization in the El Teniente porphyry?*

**Author's response:** as explained before, these dikes aren't related to mineralization at El Teniente; they are older than the late Miocene hydrothermal alteration affecting the Carlota Intrusive Complex.

**Line 103:** *Reduced paleo-stress tensors: Briefly describe here which is the methodology to separate heterogeneous data sets into homogeneous ones, since this is a very critical step to obtained robust tensors.*

**Author's response:** as explained in the text, for paleo-stress tensor calculations we used the Multiple Inverse Method, which allows to work directly with heterogeneous data sets, and to identify the different stress tensors under which the considered fault planes were active.

**Lines 277-278:** *The focal mechanism solution for the Las Melosas earthquake is quite particular, with NNW-oriented P axis, not compatible with the WNW-striking sinistral faults of the PFS.*

**Author's response:** one of the focal mechanism solutions for the Las Melosas earthquake is a subvertical fault striking N74°W, highly coincident with the PFS. However, it is correct that the sense of movement of this particular fault reactivation would be dextral strike-slip, not sinistral as was the predominant sense of movement during the Mio-Pliocene. We added a mention to this point in the new version of the text.

Comments about the figures:

**Figure 1:** *add sense of displacement of normal and strike-slip faults.*

**Author's response:** the faults shown in this figure, in particular de fundamental basement fault, can have multiple reactivations trough time with different kinematics, determined by variations on the orientation and relative magnitudes of the principal stresses. Because of this, it is not possible to assign a specific sense of movement to the faults shown in the diagram.

**Figure 2:** *Improve the location map (a) to show the main tectonic characteristics of the study area. Add lat- long in the map from Figure 1b.*

**Author's response:** done, as suggested by the reviewer.

**Figure 3:** *I suggest that the authors replace the red lines with a semi-transparent polygon.*

**Author's response:** done, as suggested by the reviewer.

**Figures 3 and 5:** *These figures can be integrated into one. Add lat-long, volcanoes, rivers, and localities (for example. Santiago and Rancagua cities, San José de Maipo, etc)*

**Author's response:** we decided to leave them as separate figures, but showing the Landsat satellite image in Figure 3 and the geological map in Figure 5. In Figure 3, we labelled the cities of Santiago and Rancagua, the Maipo river valley, and the Maipo volcano, as suggested.

**Figures 9, 11, 12 and 13:** *These figures will benefit a lot if, instead of presented the satellite image again, the authors add a geological map and locate the stereoplots in the borders of the map (not inside it).*

**Author's response:** we replaced the satellite image by the geological maps in all these figures, as suggested by the reviewer.

**Referee 2: anonymous**

**About the text organization:**

**Comment:** *1) The Introduction should be broadened by emphasising the importance of a multidisciplinary approach in characterising the evolution (in time and space) of lithospheric-scale faults. Moreover, it should be clarified how it is possible to link structural information from exposed structures to deeply-seated tectonic lineaments. Some examples around the world should be mentioned for reference. Moreover, it should be emphasised the importance of constraining the time of tectonic evolution for the lithospheric-scale faults, to link a tectonic event to a hydrothermal/magmatic/volcanic process.*

**Author's response:** the introduction was enhanced, including all the topics mentioned in the referee's comment.

**Comment:** *2) The Geological Background should be improved. In particular, I propose to better describe: (i) the subduction framework controlling the geodynamics of South America; (ii) the tectonic setting of South America (Western Cordillera, Eastern Cordillera, Coastal Range); (iii) the*

*tectonic relationships between on-shore and off-shore occurrence of regional fault systems. This is recommended to better follow the tectonic framework illustrated within paragraph #5.3 and figures 16-17.*

**Author's response:** in the new version of the text, these points were all included in the Introduction and the Geological Background.

**Comment:** 3) *Results. I believe this paragraph should be improved by reorganising the text in three sub-paragraphs: a. #4.1 - Study areas (lines 113-116; lines 128-142) b. #4.2 – Structural analysis (lines 110-114; 144-165) c. #4.3 - U-Pb geochronology (lines 117-127; lines 532-538) Therefore, Figures 4 to 11 should be renumbered accordingly.*

**Author's response:** following the referee's suggestion, the U-Pb geochronology results are now presented as a separate sub-section, after the description of the different sectors into which the study area was subdivided, within the Results chapter.

**About data presentation and interpretation:**

**Comment:** 1) *I recommend providing structural constraints for the kinematics of the measured faults. The authors mentioned the faults are characterized by "low pitch angles, indicating predominantly strike-slip movements" (line 165). It is important to document what is reported in lines 203-204 (Syn-mineral displacement of the faults was mainly dextral for ENE to NE-striking faults, sinistral for WNW-striking faults, and sinistral-reverse for NNW-striking faults). Figure 4, alone, does not provide enough information.*

**Author's response:** regarding the first point (low pitch angle), we added a reference to Fig. 10, which shows the pitch angle of the slickenlines for all the measured fault planes. Regarding the preferred orientation of faults with different kinematics, we added a new figure (Fig. 16 in the new version of the manuscript) showing the strike of faults with a sinistral and dextral component, as suggested.

**Comment:** 2) *Within the dynamic analysis, it should be clarified that the orientation of  $\sigma_1$  should bisect the acute angle between the two system faults (sinistral WNW-ESE-striking faults and dextral ENE-WSW-striking faults) that are considered conjugate (lines 201-202) by the authors. Therefore, the resulting  $\sigma_1$  should be more E-trending.*

**Author's response:** please see our response to Comment 5) of Referee 1, which refers to this same topic.

**Comment:** 3) *The relationships between the fault system and magmatic/hydrothermal products are not clear to me. Are the hydrothermal veins syn-kinematic to the conjugate fault systems? Do you have constraints about the ages of dikes? Is it possible to consider more than one generation of dikes (at least for those that are misoriented to the estimated stress regime)?*

**Author's response:** regarding the first question, yes, hydrothermal veins are syn-tectonic. In the new version of the manuscript, we specifically mention this when describing the San Pedro de Nolasco veins, and we also included in Fig. 4 field photographs of the main veins, to illustrate its syn-tectonic character. Regarding the age of dikes, as mentioned in a similar comment by Referee 1 (comment 4), we included a more detailed discussion about the timing of their emplacement,

and why we can assign them a middle to late Miocene age. Regarding the second question, yes, it is possible that there were several generations of dikes emplaced along the PFS, within the middle to late Miocene timeframe. We now explicitly mention this in the text.

Regarding the minor comments mentioned in the supplement, all of the corrections and suggestions were incorporated to the new version of the manuscript, with the following exceptions:

**Line 94:** *I would like to remove Figure 4 from here, as it is part of the results from structural work.*

**Author's response:** we would prefer to leave the reference to Figure 4 in the Methodology section, as it illustrates to the reader the different types of kinematic criteria which were used to establish the sense of movement of faults.

**Lines 182 to 186:** *this part should move in the Results paragraph.*

**Author's response:** following the suggestion of the Topical Editor, all the section regarding paleo-stress tensor calculations was moved to the Discussion chapter.

Comments about the figures:

**Figure 3:** *I would put here a geological map as the background. The Landsat image is not useful to the aim of the paper. Moreover, the legibility of the fault pattern (black lines) is hindered by the coloured image.*

**Author's response:** we decided to leave the satellite image in this particular figure, and we added labels to show geographical features useful for the readers (main cities, valleys, the Maipo volcano), as suggested by Referee 1. However, we replaced the satellite image by the geological map in all the subsequent figures.

**Figure 4:** *these pictures need for the orientation. How was the sense of movement estimate for pictures (a) and (b)?*

**Author's response:** the picture orientation was added to the figure, as suggested by the Referee. The sense of movement was estimated from the geometry of steps in syn-tectonic epidote and actinolite, and from its crystallization in strain fringes. This explanation was added to the figure caption.

**Figure 5:** *same comment as before. I would replace the Landsat image with a geological map. The same for next figures*

**Author's response:** done as suggested by the reviewer.

**Figure 7:** *please, provide picture orientation and add more labels/lines to improve the legibility.*

**Author's response:** done as suggested by the reviewer.

# The Piuquencillo Fault System: a long-lived, Andean-transverse fault system and its relationship with magmatic and hydrothermal activity

José Piquer<sup>1</sup>, Orlando Rivera<sup>2</sup>, Gonzalo Yáñez<sup>3,4</sup>, Nicolás Oyarzún<sup>1</sup>

<sup>1</sup>Instituto de Ciencias de la Tierra, Universidad Austral de Chile, Valdivia, 5090000, Chile

5 <sup>2</sup>Minera Peñoles de Chile, Santiago, 8320000, Chile

<sup>3</sup>Departamento de Ingeniería Estructural y Geotécnica, Pontificia Universidad Católica de Chile, Santiago, 8320000, Chile

<sup>4</sup>Núcleo Milenio Trazadores de Metales (NMTM), Santiago, 8320000, Chile

*Correspondence to:* José Piquer (jose.piquer@uach.cl)

**Abstract.** Lithospheric-scale fault systems control the large-scale permeability in the Earth's crust and lithospheric mantle, and its proper recognition is fundamental to understand the geometry and distribution of mineral deposits, volcanic and plutonic complexes and geothermal systems. However, their manifestations at the current surface can be very subtle, as in many cases they are oriented oblique to the current continental margin and to the axis of the magmatic arc, can be partially obliterated by younger, arc-parallel faults, and can also be covered by volcanic and sedimentary deposits, through which the fault might propagate vertically.

15 The Piuquencillo Fault System (PFS) is a proposed lithospheric-scale fault system, located in the Main Cordillera of Central Chile. Here we present the results of the first detailed field study of the PFS, based on structural data collected at 82 structural stations distributed across all the Western Main Cordillera. The first published U-Pb zircon ages for the La Obra batholith, which is bounded to the south by the PFS but it is also affected by younger reactivations of it, were obtained. They yielded 20.79 ± 0.13 Ma (granodiorite) and 20.69 ± 0.07 (monzogranite). Statistical analysis of fault plane data shows that the presence of the PFS is reflected on a strong preferred NW to WNW strike, with variable dip directions, evident from the analysis of the total fault plane population and also from individual segments of the PFS. In some segments, the presence of major NE to ENE-striking faults which intersect the PFS is also reflected in the preferred orientation of fault planes. Preferred orientations of hydrothermal veins, breccias and dikes show that both the PFS and some ENE-striking faults were capable of ~~channeling~~ channelling hydrothermal fluids and magma. Kinematic and dynamic analysis of fault-plane data reveals that most of the PFS was reactivated with sinistral ± reverse kinematics during the Neogene, under a strike-slip to transpressive regime with E- to ENE-trending shortening direction ( $\sigma_1$ ). Detailed kinematic and dynamic analyses were completed for various segments of the PFS and also for the different rock units affected by it.

25 This study supports the concept that the PFS is a lithospheric-scale fault system, which strongly controlled deformation and the flow of magmas and hydrothermal fluids during the Neogene. The PFS forms part of a larger, margin-transverse structure, the Maipo Deformation Zone, a continental-scale discontinuity which cut across the entire Chilean continental margin, and which has been active at least since the Jurassic.



## 1 Introduction

Large-scale permeability of the crust and lithospheric mantle, is controlled by the presence of ~~L~~-lithospheric-scale fault systems control the large scale permeability of the crust and lithospheric mantle (McCuaig and Hronsky, 2014). ~~This implies that their characterization is, and their proper recognition is~~ fundamental to understand the distribution and geometry of magmatic-hydrothermal systems and the mineral deposits, volcanic complexes and geothermal systems with which they might be related. However, ~~their surface expression of these type of structures is often manifestations in the present day surface can be~~ very subtle. ~~As they correspond to ancient features,~~ as in many cases they are oriented oblique to the axis of younger magmatic arcs and can be obliterated by younger, arc-parallel faults. ~~They and~~ might also be covered by volcanic and sedimentary deposits through which the fault has to propagate vertically (Fig. 1). ~~These difficulties can be overcome with a multidisciplinary approach, combining detailed, field-based structural mapping with geologic observations at different scales and various types of geophysical datasets; such an approach has led to the recognition of this type of lithospheric-scale structures in different geological settings, improving our understanding about their complex reactivation histories and their relationship with magmatic-hydrothermal activity (e.g., Chernicoff et al., 2002; Gow and Walshe, 2005; Cembrano and Lara, 2009; Acocella et al., 2011; Lanza et al., 2013; Richards et al., 2013; Fox et al., 2015; Febbo et al., 2019).~~

In the Chilean and Argentinean Andes, several authors have proposed the existence of pre-Andean, lithospheric-scale structures which are oblique to the N-trending present-day continental margin (Salfity, 1985; [Rivera and Cembrano, 2000](#); Chernicoff et al., 2002). It has been suggested that this pre-Andean structures control the distribution of fossil and active magmatic-hydrothermal centres, including those related to porphyry deposits in northern and central Chile ([Rivera and Cembrano, 2000](#); Richards et al., 2001; Piquer et al., 2016; [Yáñez and Rivera, 2019](#)) and volcanic and geothermal systems in the southern part of the country (Cembrano and Lara, 2009). [Morphologic and seismic data evidence the offshore continuation of these fault systems \(Hicks and Rietbrock, 2015\)](#). This type of structures also bound uplifted basement blocks, and acted as basin-bounding faults during various episodes of extensional deformation during Andean evolution (Yáñez and Rivera, 2019). However, for most of these structures their field expression remains unclear, as they have been inferred from different types of lineaments or alignments, from geophysical data sets and from abrupt regional-scale discontinuities of N-trending geological units. Here we present the first field-based study of the Piuquencillo Fault System (PFS), a proposed lithospheric-scale structure present in the Andes of central Chile, including a characterization of its kinematics and related paleo-stress tensors, for each individual segment of the PFS. Then we complement our results with different types of geological and geophysical data, [including U-Pb zircon dating of plutonic units bounded by the PFS](#), to provide an integral characterization of this fault system. ~~We also, and we~~ discuss the relevance of this long-lived structure during Andean evolution up to this day, including its role as a pathway for magmas and hydrothermal fluids, and its potential seismic hazard for Chile's most densely populated area.

## 2 Geological background

The Andes of central Chile can be subdivided into two parallel, N-trending ranges, the Coastal and Main Cordilleras (Fig. 2).

65 The Main Cordillera ~~of central Chile (Fig. 2)~~ was the position of the Paleogene-Neogene magmatic arc, related to active subduction of the oceanic Farallon/Nazca plate below the western margin of the South American continent (Pardo Casas and Molnar, 1987; Charrier et al., 2002). Consequently, the Main Cordillera at this latitude ~~is~~ is composed mostly of Cenozoic volcanic and intrusive rocks, with subordinate sedimentary intercalations. The evolution of this magmatic arc is characterized by the opening and subsequent inversion of the Abanico Basin (Charrier et al., 2002), an intra-arc volcano-tectonic basin  
70 formed between the Late Eocene and the Early Miocene and inverted in specific, short-lived pulses of ~~compressive~~ contractional deformation since the Early Miocene (Charrier et al., 2002; Piquer et al., 2017). The widespread volcanic and sedimentary deposits accumulated during the extensional stages of the basin have been ~~grouped~~ grouped into two main stratigraphic units: the Abanico Formation (Aguirre, 1960; Thomas, 1953), in the area to the east of the city of Santiago (Fig. 2), and the Coya-Machalí Formation (Klohn, 1960) in the mountain regions to the south of it (Fig. 2). The thickness of these units is  
75 highly variable, although it can reach up to 5 km (Piquer et al., 2017). Volcanic and sedimentary deposits were accumulated in extensional basins, bounded by normal faults. Main basin-bounding faults were N-striking; they dip to the W in the eastern basin margin (El Fierro-Las Leñas-El Diablo faults, Charrier et al., 2002; Farías et al., 2010) and to the E in the western margin (Infiernillo and Pocuro-San Ramón faults, Farías et al., 2010). Individual segments of the Abanico Basin, in turn, were bounded by arc-oblique, NW- and NE-striking fault systems, also active as predominantly normal faults during this period (Piquer et  
80 al., 2015, 2017).

Tectonic inversion since the Early Miocene was associated with a decrease in the rates of volcanic output and with the emplacement in the upper crust of a series of Miocene to early Pliocene plutons (Fig. 2). Volcanic rocks accumulated during tectonic inversion are grouped into the Farellones Formation in the area to the east of Santiago (Klohn, 1960), and the Teniente Volcanic Complex (TVC) towards the south (Godoy, 1993; Kay et al., 2005; Fig. 2). The final stages of Neogene compressive  
85 deformation, crustal thickening and Neogene magmatism in the late Miocene – early Pliocene produced large produced the growth of differentiated, upper-crustal magmatic-hydrothermal complexes, which led to the formation of two giant porphyry Cu-Mo deposits: Río Blanco-Los Bronces and El Teniente (Fig. 2). After the formation of these two mineral deposits, the magmatic arc migrated ~40 km towards the east. During tectonic inversion, the N-striking, basin-bounding faults of the Abanico Basin were reactivated as high-angle reverse faults (Charrier et al., 2002; Giambiagi et al., 2003; Farías et al., 2010),  
90 while the arc-oblique fault systems which segmented the basin, were reactivated as strike-slip faults with a variable reverse component (Piquer et al., 2015, 2016).

The NW to WNW-striking PFS was defined during regional-scale geological studies around the El Teniente Cu-Mo porphyry deposit ~~by (Rivera and Cembrano, 2000; Rivera and Falcon, (2000).~~ These authors indicated that the fault has an average strike of N60°W, dipping 70-80° towards the south. It was proposed that the fault acted as a basin-bounding fault during extensional  
95 deformation related to the opening of the Abanico Basin. ~~The~~ The Coya-Machalí Formation, which according to the authors has

a larger sedimentary component than the also syn-extensional Abanico Formation, appeared to be present only to the south of the PFS. A set of sheeted dikes was emplaced later along different branches of the PFS. Later studies, based on U-Pb zircon geochronology and whole-rock geochemistry, confirmed that the PFS constitute a major boundary between two contrasting segments of the Abanico Basin (Piquer et al., 2017; Fig. 2). The two segments are, characterized by different stratigraphic units and also showing major differences in their tectonic evolution and exhumation history. In the northern segment, which contains the Río Blanco-Los Bronces porphyry, stratigraphic units correspond to the Abanico Formation (~34-22 Ma) and the Farellones Formation (~22-16 Ma), commonly separated by progressive-angular unconformities. In the southern segment, the Abanico Formation is also present, but is covered by the younger Coya-Machalí Formation (23-13 Ma), which is in turn covered by the sub-horizontal volcanic deposits of the TVC (13-6 Ma; Piquer et al., 2017). Rare Earth Elements (REE) patterns in igneous rocks also show major differences between the northern and southern segments (Piquer et al., 2017); This can be observed in the depletion of HREE documented in lava flows of the Farellones Formation-, not observed in the coeval deposits of the Coya-Machalí Formation-, and also in middle Miocene plutons emplaced in both segments, which also show a clearly stronger depletion of HREE and steeper REE patterns in the northern segment. This suggest that the northern segment was affected by compressive deformation and crustal thickening earlier than the southern segment.

### 3 Methodology

Figure 3 shows the distribution of structural stations within the PFS and surrounding areas. Data was collected~~captured~~ during three field campaigns, between 2016 and 2018. From the 82 structural stations shown in Fig. 3, 240 fault planes were measured, 54 of them containing kinematic information. The parameters measured in each fault plane were strike and dip, rake of striation, thickness of the fault and its damage zone-, hydrothermal mineral infill (when present) and, when possible, sense of movement based on different kinematic criteria for brittle faults (Fig. 4). Most kinematic indicators are related to the geometry of syn-tectonic hydrothermal minerals (Fig. 4). When syn-tectonic minerals were absent, sense of movement was established by RM and P-only criteria (Petit, 1987; Fig. 4) and by offset markers. Additionally, the orientation of 50 dikes and 109 veins and hydrothermal breccias were obtained. The complete structural database is available as Supplementary material.

Preferred orientations of faults, dikes and veins were analyzed using the software Stereonet (Allmendinger et al., 2012). Kinematic and dynamic analyses of the fault plane database were also completed. The aim of the first one is to establish the orientation of the compression and tension axes for each individual fault plane and the average kinematic axes (shortening, stretching and intermediate axes) for different fault populations. This was achieved using the FaultKin software (Allmendinger et al., 2012). Regarding the dynamic analysis, the Multiple Inverse Method (Yamaji, 2000) was used to calculate the orientation of paleo-stress tensors from the inversion of fault-slip data. The advantage of this method is that it allows the identification of separate stress states from heterogeneous data sets. A stress state is defined by four parameters: the orientation of the three principal stresses ( $\sigma_1, \sigma_2, \sigma_3$ ) and the stress ratio  $\Phi = (\sigma_2 - \sigma_3)/(\sigma_1 - \sigma_3)$ . The stress ratio varies from 0 to 1, and describes the shape of the stress ellipsoid.

Two U-Pb LA-ICP-MS zircon ages were obtained at the Geochronology Laboratory of SERNAGEOMIN, the Chilean geological survey. Analytical procedures are detailed in Appendix 1.

#### 130 4 Results

The structural database obtained from the 82 structural stations was used to establish the preferred orientations of fault planes, veins and dikes, and also to complete kinematic and dynamic analyses with the aim of establishing the prevailing strain axes and stress tensors in different segments of the PFS and ~~conjugate other nearby~~ faults, and during successive reactivation events. To achieve this aim, the study area was subdivided into five sectors (Fig. 5), each of them characterized by specific lithologies and structural patterns.

135 The Clarillo-La Obra sector (Fig. 5) includes structural stations located along one of the main WNW-striking branches of the PFS; the affected lithologies correspond to the early Miocene La Obra batholith and the Abanico Formation volcanic rocks. ~~Two new U-Pb zircon ages were obtained for this study (Table 1, analytical data in Appendix 2), from samples collected from different facies of the La Obra batholith. The La Obra batholith corresponds to a major intrusive complex which is bounded to the south by the PFS but it is also affected by younger reactivations of it, and from which no previous U-Pb crystallization ages have been documented. Tera-Wasserburg plots for the dated samples are shown in Fig. 6. The two samples are representative of the two main facies of the La Obra batholith. Sample FP01~~ Two main facies of the batholith were recognized. One of them corresponds to an equigranular, medium- to coarse-grained granodiorite, with abundant, biotite-rich granodiorite, and minor hornblende. Some biotite crystals show weak chlorite alteration at their margins. The granodiorite contains common rounded enclaves of diorite composition, composed of fine-grained plagioclase, hornblende and magnetite. ~~which~~ This is the most typical lithofacies of the intrusive complex. ~~This sample yielded an age of  $20.79 \pm 0.13$  Ma. Sample FP03~~ The second major lithofacies correspond to a hornblende-rich quartz-monzogranite, with minor biotite. Both mafic minerals are variably altered to chlorite. Graphic texture of alkali feldspar and quartz is common. ~~which~~ This unit is finer grained than the granodiorite, and it is exposed at the westernmost outcrops of the batholith. ~~The calculated age of  $20.69 \pm 0.07$  Ma from this sample is almost identical to the main granodioritic body. These ages confirm that La Obra is the southernmost early Miocene intrusive complex of central Chile; to the south of the PFS, all the outcropping plutonic complexes in the Main Cordillera are middle Miocene or younger (Piquer et al., 2017, and references there in).~~

145 The Piuquencillo alto and Piuquencillo-Claro sectors (Fig. 5) are located in the Piuquencillo river valley, where the PFS was defined (Rivera and Falcon, 2000). In the Piuquencillo alto sector, the main lithological unit are different intrusive facies of ~~the late Miocene plutons~~ Carlota Intrusive Complex (CIC), which is ~~are~~ emplaced in volcanic rocks of the middle Miocene Teniente Volcanic Complex TVC. The main facies of the CIC is a hornblende- and biotite-rich granodiorite, with variable degrees of hydrothermal alteration. This facies was dated by Kurtz et al. (1997) at  $8.7 \pm 0.3$  Ma ( $^{40}\text{Ar}/^{39}\text{Ar}$  in biotite). Because of the evidences of relatively high-temperature hydrothermal alteration (secondary minerals such as epidote, chlorite, actinolite and muscovite), it is likely that this age reflects the time of hydrothermal activity, not of magmatic crystallization. Diorites, quartz-diorites, monzodiorite porphyries and quartz-monzonites were also observed within the CIC. The Piuquencillo-Claro

sector, in turn, is dominated by volcanic and volcanoclastic rocks of the Abanico and Coya-Machalí Formations, intruded by small-scale andesitic and daci-andesitic stocks and dikes. According to regional-scale stratigraphic interpretations (Piquer et al., 2017) the PFS correspond to the transition zone between these two units, with the Coya-Machalí Formation present only towards the south of this structure. There are no absolute ages for the dike sets, but because of the age of their host rocks, they are post-early Miocene in age. No dikes of this type were observed cross-cutting the altered CIC rocks in the Piuquencillo Alto sector, from which we infer they were emplaced before the late Miocene. However, several individual generations of dikes might have been emplaced during this timeframe, and they might have acted as feeder for the Teniente Volcanic Complex.

The San Pedro de Nolasco and Maipo sectors are located along a less notorious, WNW-striking branch of the PFS, and also contain traces of major NE-striking faults (Fig. 5). The San Pedro de Nolasco sector in particular includes the Ag-Pb-Zn-Cu vein system of the same name. The strike of individual veins varies from ENE to WNW, but the whole vein system defines a WNW-trending belt, 1.5 km long and 200 m wide. The veins are composed of quartz, calcite and barite with a sulphide ore of galena, sphalerite, tennantite/tetrahedrite, chalcocopyrite and bornite (Leal, 2018), and they are syn-tectonic, as demonstrated by several evidences of hydrothermal mineral crystallization during fault slip (Fig. 4). The polymetallic veins of San Pedro de Nolasco are emplaced in volcanic rocks of the ~~Teniente Volcanic Complex~~ TVC, which in the area overlay volcanic rocks of the Farellones Formation (Fig. 67). From this, a maximum middle Miocene age can be assigned to the vein system. Considering that the youngest evidences of hydrothermal activity in the Neogene magmatic arc of central Chile occur at ~4 Ma (Maksaev et al., 2004; Deckart et al., 2013, 2014), the age of the vein system can be constrained to the middle Miocene – early Pliocene. The Maipo sector, in turn, contains mostly Abanico Formation volcanic rocks, intruded by small-scale stocks and dikes, some of them probably related to the middle Miocene San Gabriel pluton, located towards the north.

#### **4.1 U-Pb zircon dating**

Two new U-Pb zircon ages were obtained for this study (Table 1, analytical data in Appendix 2), from samples collected from different facies of the La Obra batholith, from which no previous U-Pb crystallization ages have been documented. Tera-Wasserburg plots for the dated samples are shown in Fig. 7. The two samples are representative of the two main facies of the La Obra batholith: sample FP01 comes from the biotite-rich granodiorite, while sample FP03 comes from the hornblende-rich quartz-monzonite. The granodiorite sample yielded an age of  $20.79 \pm 0.13$  Ma. The calculated age of the quartz-monzonite, in turn, is  $20.69 \pm 0.07$  Ma, almost identical to the main granodiorite body. These ages confirm that La Obra is the southernmost early Miocene intrusive complex of central Chile; to the south of the PFS, all the outcropping plutonic complexes in the Main Cordillera are middle Miocene or younger (Piquer et al., 2017, and references there in).

#### **4.12 Preferred orientations**

Figure 8 illustrates the preferred orientations of dikes/main intrusive contacts, veins/main hydrothermal breccia contacts, and faults.

Dikes and intrusive contacts, and also veins and hydrothermal breccias show ~~strike~~trends varying from ENE to NNW, with a remarkable absence of strikes approaching a N-S orientation. Regarding orientation of fault planes, the strong influence of the PFS is clearly visible, with a remarkable WNW preferred orientation, parallel to the general tendency of the PFS. Also visible is a secondary trend of ENE-striking fault planes, and a minor group of NNW-striking faults. Similar to the case of the veins and hydrothermal breccias, there is a remarkable scarcity of N-S striking fault planes.

Figure 9 shows the preferred orientations of fault planes for the five different sectors into which the study area was subdivided for statistical analyses. Although the presence of large populations of WNW-striking fault planes related to the PFS is evidenced in all the five sectors, some remarkable differences are visible between them. The Piuquencillo-Claro sector, where the PFS was defined, shows the strongest dominance of WNW-striking fault planes. The Piuquencillo Alto and San Pedro de Nolasco sectors clearly show the influence of an ENE-striking fault system, apart from the PFS. The Clarillo-La Obra sector marks the presence of a NNE-striking set of fault planes, while in the Maipo area, the influence of a NE-striking fault system is evident, which probably correspond to the Yeso Valley ~~F~~fault ~~S~~system (Fig. 2), a major NE-striking, dextral strike-slip fault.

In 54 fault planes it was possible to obtain reliable kinematic information. A variety of syn-tectonic hydrothermal minerals were observed, including tourmaline, calcite, hematite, epidote and actinolite (Fig. 4). They are particularly common within and in the vicinity of plutonic complexes. The orientation of all the 54 fault planes, their slickenlines and sense of movement are shown in Fig. 10, while Fig. 11 shows the same information for each individual sector. Clarillo-La Obra sector is not shown, as no reliable kinematic data was obtained in this area. Preferred orientations of fault planes with kinematic information (Figs. 10, 11) are similar to the ones obtained from the total fault plane database (Figs. 8, 9), with a strong WNW preferred orientation, a secondary group striking ENE, and a minor population of fault planes striking NNW. Slickenlines most commonly show low pitch ~~angles~~values (Fig. 10), indicating predominantly strike-slip movements.

## 5 Discussion

### 5.1 Kinematic and dynamic analysis

When considering all the 54 fault planes for which there is kinematic information available, it is evident that the sense of movement of most of the faults is consistent with fault activity under a strike-slip regime, with ~~E-W to ENE~~-directed, sub-horizontal shortening and N-S to NNW-directed~~ing~~, sub-horizontal stretching. This is shown by the orientation of the average pressure and tension axis in the kinematic analysis and by the main clusters of  $\sigma_1$  and  $\sigma_3$  in the dynamic analysis (Fig. 10). We interpret this as the predominant regional stress state during the middle Miocene to early Pliocene, considering the ages of the different rock units affected by the faults, and the age range of hydrothermal activity in the Neogene magmatic arc of central Chile, which constrains the age of syn-tectonic mineral fibres used to obtain kinematic information in fault planes. However, the kinematic analysis (Fig. 10) shows an important dispersion of individual pressure and tension axes, suggesting a relatively heterogeneous deformation, in which the movement of several fault planes is not compatible with the average shortening (pressure) and stretching (tension) axes. The dynamic analysis, using the Multiple Inverse Method (Fig. 10), allows the

225 distinction of secondary clusters of  $\sigma_1$  and  $\sigma_3$ , both of them vertical, showing that some groups of fault planes were active under extensional and compressional conditions respectively.

As discussed before, and shown by Figure 8, most of the measured fault planes have a WNW orientation, while the veins are more evenly distributed between WNW and ENE orientations. This could be related to the predominant ENE trend of  $\sigma_1$ : as the ENE faults are more parallel to  $\sigma_1$ , they are more efficient as fluid pathways, in contrast to WNW to NNW-striking faults, which are at higher angles relative to  $\sigma_1$  and require higher fluid pressure or transient stress ~~reversals-relaxation~~ to open and allow the circulation of fluids.

Similar kinematic and dynamic analyses were completed for the five sectors shown in Figure 5, and also for different lithological units. The latter was done to explore temporal variations in the stress state and strain axis, by looking at the variability in the results of the analysis for faults cross-cutting rocks of different ages. The lithological units considered were the Abanico and Coya-Machalí Formations (late Eocene – middle Miocene); ~~t~~The Farellones Formation (early to middle Miocene) and the Teniente Volcanic Complex (middle to late Miocene); subvolcanic intrusions (middle to late Miocene); and the Miocene plutons. The results of this analyses are presented in Figures 12 to 15.

The kinematic and dynamic analysis of fault plane data by sector shows some remarkable differences between the upper and lower part of the Piuquencillo river valley. In the upper part of the valley (Piuquencillo alto), faults were active under a pure strike-slip regime (Fig. 13), while in the lower part (Piuquencillo-Claro), a transpressive (transitional between strike-slip and compressive) tectonic regime was predominant, showing very low  $\Phi$  values and a large variability in the orientation of  $\sigma_3$  (Fig. 13). This could be reflecting a trend from purely strike-slip regime in the central part of the Abanico/Coya-Machalí basin, to a transpressive regime predominant closer to the basin margins, a feature already observed in regional studies (Piquer et al., 2016) and which might be due to an excess of gravitational potential energy in the central part of the Main Cordillera, at the axis of the Paleogene-Neogene magmatic arc.

When interpreting the results of stress tensor calculations from the inversion of fault slip data, a possibility which has to be considered is that stress tensor rotations might occur in the vicinity of major faults, although the expected patterns of stress rotation are still a matter of debate (Hardebeck and Michael, 2004; Famin et al., 2014). If these stress tensor rotations occurred at the PFS, then part of our calculations might not represent a regional stress field, but a local stress tensor acting only in and around the fault traces. The dynamic analysis by sector, however, suggests that this is not the case. The Piuquencillo Alto and Piuquencillo-Claro sectors cover areas around the main traces of the PFS, while the Maipo sector is located further away from it (Fig. 13). In these three sectors, the direction of maximum horizontal compression is similar (E-W to slightly ENE), without any evidence of rotations occurring around the traces of the PFS. The results obtained are also consistent with regional calculations of the Miocene – early Pliocene stress field in central Chile (Piquer et al., 2016). All of this is consistent with the fact that none of the cropping-out branches of the PFS is individually a major fault; the strain associated to each of them is of small magnitude, so no major perturbations of the stress tensor are expected around them.

When considering the kinematic and dynamic analysis by lithological units, it is observed that the largest variability in the orientation of the principal stresses is observed in the volcanic units (Fig. 15), probably reflecting local variations in the stress

state. The tectonic (far-field) stress tensor is more clearly defined in the intrusive units. The differences in the  $\Phi$  value (Fig. 15) directly reflect the geographic position of the intrusive units: the predominant stress tensor calculated for faults in the Miocene plutons is identical to the one calculated for the Piuquencillo alto sector (Fig. 13), while the stress tensor calculated for subvolcanic intrusions is very similar to the one calculated for the Piuquencillo-Claro sector, where most of those intrusions are located.

## 5.2 Fault orientations and the flow of magmas and hydrothermal fluids

As discussed before and shown by Figure 8, it is evident that both WNW-striking faults, belonging to the PFS, and ~~conjugate~~ ENE-striking faults were capable of ~~channeling~~ channelling magmas and hydrothermal fluids, as reflected in the preferred orientations of dikes and, particularly, hydrothermal veins and breccias. Syn-mineral displacement of the faults was mainly dextral for ENE- to NE-striking faults ~~and~~, sinistral for WNW-striking faults, ~~and sinistral reverse for NNW-striking faults~~ (Fig. 16). ~~This suggests that the PFS and the ENE-striking faults acted broadly as conjugate faults under the prevailing middle Miocene – early Pliocene stress tensor. However, they are not oriented at the ideal angle with respect to  $\sigma_1$  expected in intact rocks, with the ENE-striking faults being more parallel to  $\sigma_1$  than the fault planes of the PFS. The reason for this might be that both sets of faults are part of large-scale, pre-existing fault systems (the PFS and, for the ENE-striking faults, the Yeso Valley Fault System), reactivated during the Mio-Pliocene, but not originated as conjugate structures. As also noted before, the ENE-striking faults are more parallel to the predominant orientation of  $\sigma_1$  (E-W to ENE-trending), they were the most favorably~~ favorably oriented for opening, ~~under the calculated predominant stress regime (E-W to ENE-trending  $\sigma_1$ )~~, which explains why ENE-striking veins are as common as those striking WNW, while ENE-striking fault planes are much less frequent (Fig. 8). NNW-striking fault segments of the PFS in particular are the least ~~favorable~~ favorable for opening under the predominant stress regime. This could make them highly attractive for mineral exploration, as they will tend to remain sealed for large periods of time, accumulating volatiles and allowing magmas to differentiate at depth, until fault reactivation occurs (perhaps triggered by co-seismic stress ~~reversals~~ relaxation leading to transient local extension, as suggested by Mpodozis and Cornejo, 2012) creating instant permeability along the fault and allowing the rapid (often catastrophic) ascent of differentiated magmas and hydrothermal fluids. This is very clearly observed in the Río Blanco-Los Bronces porphyry Cu-Mo cluster, in which hydrothermal breccias and dacitic porphyries are emplaced along a NNW-striking fault system, while most of the late quartz veins and andesitic dikes are emplaced along NE-striking faults, more ~~favorable~~ favorable for opening (Mpodozis and Cornejo, 2012; Piquer et al., 2015).

## 5.3 Beyond the PFS: the Maipo Deformation Zone

Our new field data demonstrate that the PFS can be traced across the entire Western Main Cordillera (~~Fig. 16~~ Fig. 17) of Central Chile, ~~confirming the proposition of Rivera and Cembrano (2000)~~. However, Yáñez et al. (2002) proposed that the PFS might be part of a larger, continental-scale discontinuity, the Maipo Deformation Zone (~~MDZ; Fig. 16~~ Fig. 17). Several recent works completed in the coastal ranges near Valparaíso (~~Fig. 16~~ Fig. 17), after the work of Yáñez et al. (2002) was published, confirm



that the PFS can be extended to the NW across the entire continental margin. Evidences for the existence of a deep, long-lived, NW-striking fault system in the coastal ranges are varied. Creixell et al. (2011) showed that different Jurassic intrusions were syn-tectonically emplaced along NW-striking faults, under both sinistral transtension and transpression, while Hernández (2006) documented primitive, Mesozoic mafic and ultramafic rocks of mantle origin emplaced along similar faults. In the same area, the structural architecture of the Upper Jurassic Antena Au vein district (Townley et al., 2000), is also dominated by NW-striking faults, which control the location of the mineralized district together with a system of conjugate, NE-striking faults. More to the SE, a similar situation occurs at the Early Cretaceous Lo Aguirre stratabound Cu deposit (~~Fig. 16~~Fig. 17): the orebody has a very strong NW elongation, while post-mineral faults strike NE (Saric et al., 2003). The latter appear to be also part of a large-scale structure, as they are on strike of a set of major NE-striking faults identified in the Western Main Cordillera (the Saladillo, Flores and El Salto fault systems, Piquer et al., 2015), in the vicinity of the Río Blanco-Los Bronces porphyry Cu-Mo cluster (~~Fig. 16~~Fig. 17). Subsequently, Rivera (2017) showed that this NW-striking fault system is associated with regional-scale geological discontinuities in the coastal ranges. To the north ~~of it~~, there is a continuous N-trending belt of Jurassic sedimentary and volcanic units (Ajial, Cerro Calera and Horqueta Formations), and Paleozoic rocks are absent. To the south, outcrops of Jurassic stratigraphic units and plutons are highly discontinuous, and the geology of the coastal ranges is dominated by late Paleozoic intrusions and isolated blocks of metamorphic rocks (SERNAGEOMIN, 2002; Rivera, 2017; see ~~Fig. 16~~Fig. 17). Yáñez and Rivera (2019) proposed the existence of a series of continental-scale discontinuities in the Chilean continental margin, which they defined as TLFs (Trans-Lithospheric Faults). The concept of a TLF is equivalent to the fundamental basement structures of McCuaig and Hronsky (2014). Even though the whole lithosphere involvement of these continental-scale structures has not been demonstrated empirically in the Andes, several lines of reasoning provide independent arguments to support this concept. In one hand, Yáñez and Rivera (2019) proposed that the origin of these deep-seated structures could be related with master and transform faults associated with ancient rifting and/or suture zones related to collisional processes. In both likely scenarios, recent analogues show the presence of deep seated structures that involve the whole lithosphere (i.e. Kuna et al., 2019; Hua et al., 2019). On the other hand, several authors have demonstrated that continental-scale deformation zones, of some hundreds of kilometres length (comparable in scale to the PFS/MDZ), are controlled by the rheology of the mantle (i.e. Bird and Piper, 1980, England and McKenzie, 1984). Moreover, numerical models, in agreement with field observations, indicate that deformation decays laterally to 1/10 of the structure length for strike-slip dominated movements (England et al., 1985), thus developing a deformation zone of 10-30 km width, similar to the PFS/MDZ. According to the interpretation of Yáñez and Rivera (2019), Lo Aguirre was emplaced at the intersection of two TLFs, at the margins of a dense crustal block observed in regional gravity data: the Valparaíso-Volcán Maipo TLF, which coincides with the Maipo Deformation Zone (including the PFS), and the Aconcagua-San Antonio TLF, which includes the NE-striking fault systems identified in Lo Aguirre and at the Río Blanco-Los Bronces district. These areas of intersection of major fundamental basement structures develop complex interference patterns dominated by abundant secondary faults and fractures, and therefore are associated with high permeability, being favorable sites for the emplacement of mineral deposits.

Also, it is common that these intersecting, continental-scale faults define wedge-shaped blocks with distinctive stratigraphy and internal deformation styles (Piquer et al., 2019).

Within the study area, at the Clarillo-La Obra and Piuquencillo/Piuquencillo-Claro sectors (Fig. 5), the PFS coincides with a major change in the deformation style of the Cenozoic infill of the inverted Abanico Basin. Towards the south, the Miocene Coya-Machalí Formation crop out, and this unit is strongly deformed by a series of tight folds and reverse faults, constituting the Cordón Perales fold and thrust belt (Rivera, 2017). The fold axes of these folds are ~~interrupted-truncated~~ by the PFS, and to the north of it, the Coya-Machalí Fm. is absent (Fig. 2) and the older, Eocene-Oligocene Abanico Formation is more gently folded.

Towards the SE of the study area, the PFS is associated with major changes in the orientation and vergence of the N- to NNE-striking fault systems that define the boundary between the Western and Eastern Main Cordillera, at the inverted eastern margin of the Paleogene Abanico Basin (~~Fig. 16~~Fig. 17; Rivera, 2017). Moreover, the seismic activity related to these arc-parallel faults is much more intense to the south of their intersection with the PFS than to the north of it, and a very large cluster of seismic activity appears at the intersection zone (see Fig. 3 of Piquer et al., 2019). ~~Nevertheless, Even though~~ we cannot rule out other reasons to explain the differences in seismic activity, among them differences in recording time window and/or differences in water percolation between both sectors. Further SE, in the Eastern Main Cordillera, the prolongation of the PFS is at least spatially related to the Escalones prospect (~~Fig. 16~~Fig. 17), a Cu skarn deposit emplaced in Lower Cretaceous marine sedimentary rocks, with a well-developed skarn alteration mineralogy, and high hypogene Cu grades (Maksaev et al., 2007). There is no published information about the local-scale structural controls on mineralization at Escalones, but the Lower Cretaceous calcareous beds strike NW, parallel to the PFS (Maksaev et al., 2007). To the SE of Escalones, the PFS follows the northern margin of the Diamante Caldera, a major Pleistocene collapse structure (Stern et al., 1984; Harrington, 1989) within which the Maipo stratovolcano (~~Fig. 16~~Fig. 17) is located.

There is also evidence that some segments of the MDZ are tectonically active. Sabaj (2008) identified and characterized potentially active faults in the Coastal ranges of central Chile. It was concluded that fault architecture in the area is dominated by NW-striking faults, intersected by different sets of NE-striking faults. At least four of the individual NW-striking faults recognized in the work of Sabaj (2008) are located within the Maipo Deformation Zone, on-strike of the PFS: the Marga-Marga, Valparaíso, Laguna Verde and Valparaíso-Curacaví faults. They were later grouped in the Valparaíso Fault System (VFS) by Del Valle (2018). Both the NW- and NE-striking faults were concluded to be potentially active by Sabaj (2008), although the NW-striking faults were considered to pose the higher risk, as their traces are more continuous and longer. It was estimated that the maximum possible magnitude ( $M_w$ ) of seismic events generated by the NW-striking faults is between 5.8 and 7.1. The seismic hazard posed by these NW-striking faults in the Andean forearc was confirmed by the activation of the Pichilemu fault, a regional-scale fault located ~140 km to the south of the MDZ, after the  $M_w$  8.8 subduction earthquake of 27 February 2010 (Farías et al., 2011; Aron et al., 2013). The Pichilemu fault was activated on 11 March, 12 days after the main interplate earthquake, and produced two main shocks,  $M_w$  6.9 and 7.0 (Farías et al., 2011; Aron et al., 2013). Focal mechanisms indicate normal movement of the SW-dipping Pichilemu fault (Farías et al., 2011; Aron et al., 2013), consistent with the

360 expected relaxation of NW-striking crustal faults (normally under compression) during the co- and post-seismic periods, as  
was also observed in the volcanic arc at the Main Cordillera (Spagnotto et al., 2015). In the Main Cordillera, there is no direct  
evidence of neotectonic activity of the PFS, but similar, WNW-striking faults have been shown to displace Quaternary terraces  
of the Maipo river, ~25 km to the north of the PFS (Lavenu and Cembrano, 2008). One of the focal mechanism solutions of  
the Las Melosas earthquake, a major (Mw 6.9) intraplate seismic event registered in 1958 in the Main Cordillera, less than 10  
km to the north of the PFS, is compatible with activity along a WNW-striking fault (Alvarado et al., 2009). If this was the case,  
it is most likely that this earthquake was generated by one of the northernmost branches of the PFS, although this particular  
365 fault reactivation would involve a dextral strike-slip sense of movement (Alvarado et al., 2009), not sinistral as was the  
predominant sense of movement during the Mio-Pliocene (Fig. 16). However, the other possible solution, represented by a  
NNE-striking fault plane, is equally plausible, considering the presence of several individual faults with NE- to NNE-strike  
near Las Melosas (Piquer et al., 2019).

370 Considering the fact that both the PFS in the Main Cordillera and the VFS in the fore-arc are potentially active, it is worth  
noting that the southern part of the city of Santiago is built on top of the MDZ, between the PFS and the VFS. The Santiago  
valley is covered by unconsolidated sedimentary and volcanic deposits (SERNAGEOMIN, 2002; ~~Fig. 16~~Fig. 17). Yáñez et al.  
(2015), based on detailed gravimetric modelling, showed that the topography of the basement of the Santiago valley presents  
large-scale breaks and scarps which coincide with the expected position of major branches of the MDZ, and also with other,  
NE-striking faults. The assessment of the neotectonic activity of the MDZ-related faults, their recurrence intervals and the risk  
375 they pose to the Santiago and Valparaíso urban areas are highly relevant topics, which require further studies and evaluation.  
As shown in ~~Fig. 16~~Fig. 17, there is a second continental-scale structural system sub-parallel to the PFS and the Maipo  
Deformation Zone, located immediately ~~to the south of it~~southward. This second fault system, from east to west, defines the  
southern boundary of the Diamante caldera, it has been well recognized at the El Teniente porphyry Cu-Mo district (Piquer et  
al., 2016; ~~Fig. 16~~Fig. 17), and it is also well defined at the Coastal ranges and plains of central Chile (SERNAGEOMIN, 2002;  
380 ~~Fig. 16~~Fig. 17), passing through the port city of San Antonio. Here we will refer to this structure as the Teniente-San Antonio  
fault system. This major fault system and the Maipo Deformation Zone might be the manifestations in the present-day surface  
of the same continental scale discontinuity at depth; however, testing this possibility is beyond the scope of this work.

There are also geophysical evidences that highlights the relevance of the PFS, the broader Maipo Deformation Zone, and also  
the Teniente-San Antonio fault system. Yáñez et al. (1998) defined the Melipilla anomaly, a large-scale, WNW-striking  
385 negative magnetic anomaly located in the coastal area of central Chile (~~Fig. 17~~Fig. 18), which coincides with the western  
segment of the Teniente-San Antonio fault system. To the north of the Melipilla anomaly, a second, NW-striking negative  
magnetic anomaly is also evident (~~Fig. 17~~Fig. 18), and coincides with the western segment of the Maipo Deformation Zone.  
These negative magnetic anomalies most likely correspond to felsic Paleozoic and Mesozoic intrusive bodies, emplaced along  
these long-lived fault systems.

390 Finally, a different type of manifestation of these continental-scale structures might have been observed during the Valparaíso  
seismic sequence of 2017 (Nealy et al., 2017). The distribution of the hypocenters of the multiple earthquakes registered during

this event (Fig. 17 Fig. 18) shows a clear NW alignment, and is neatly bounded by the submarine prolongation of the Maipo Deformation Zone and the Teniente-San Antonio fault system. The earthquakes are strongly concentrated at the plate boundary mega-thrust (Nealy et al., 2017), so they were not generated by the activation of crustal faults. However, the remarkable spatial relationship between earthquake distribution and large-scale faults in the continental lithosphere shown in Fig. 17 Fig. 18, might indicate the existence of a still poorly understood feedback mechanism between large-scale, trans-lithospheric discontinuities in the upper plate and the distribution of subduction-related earthquake sequences at the plate boundary.

## 6 Conclusion

- The continuity and surface expression of the PFS across all the Western Main Cordillera is confirmed
- 400 - During the middle to late Miocene, the PFS was active with sinistral to sinistral-reverse kinematics, under a strike-slip to transpressive tectonic regime with sub-horizontal, E-W to ENE-trending  $\sigma_1$
- Both the PFS and conjugate, ENE-striking faults, channelled the flow of magmas and syn-tectonic hydrothermal fluids. The ENE-striking faults were more efficient pathways for hydrothermal fluids than the PFS
- A lower Miocene crystallization age (20.9-20.6 Ma, U-Pb in zircons) is confirmed for the La Obra pluton, which is  
405 bounded to the south by the PFS
- The PFS corresponds to the expression in the Western Main Cordillera of a continental-scale fundamental basement structure (Fig. 16 Fig. 17), which has been called the Maipo Deformation Zone or the Valparaíso-Volcán Maipo trans-lithospheric fault. This structure has been active at least since the Jurassic, controlling the flow of magmas and hydrothermal fluids, and at least some of its segments are still tectonically active today
- 410 - The surface expression of pre-Andean, lithospheric-scale fault systems is often very subtle, but they can be characterized through multidisciplinary studies involving, among others, detailed structural field work and geophysical interpretations. The study of this type of long-lived fault systems is a relevant task, as they strongly control the distribution and geometry of both fossil and active magmatic-hydrothermal systems, and they can be reactivated with different kinematics during the seismic cycle; the seismic hazard associated with this structures requires more detailed evaluations

## 415 Author contribution

José Piquer and Nicolás Oyarzún completed the field work and the analysis of fault plane data. Orlando Rivera participated actively in the interpretation of structural and stratigraphic data, providing inputs based in his earlier works at the Piuquencillo Fault System. Gonzalo Yáñez completed the geophysical interpretations. José Piquer prepared the manuscript with important contributions from the co-authors, mainly Orlando Rivera and Gonzalo Yáñez.

## 420 Acknowledgments

Founding for the first two field campaigns completed as part of this work came from the DID project S-2016-32, an internal research project from Universidad Austral de Chile titled “El Sistema de Falla Piuquencillo: evolución y control sobre el

emplazamiento de sistemas hidrotermales”. The logistics and costs involved on the third field campaign were covered by the Rio Tinto mining company. All the analytical costs were covered by DID project S-2016-32.

## 425 **References**

- [Acocella, V., Gioncada, A., Omarini, R., Riller, U., Mazzuoli, R., and Vezzoli, L.: Tectonomagmatic characteristics of the back-arc portion of the Calama–Olacapato–El Toro Fault Zone, Central Andes, \*Tectonics\*, 30, TC3005, doi: 10.1029/2010TC002854, 2011.](https://doi.org/10.1029/2010TC002854)
- Aguirre, L.: Geología de los Andes de Chile Central, Provincia de Aconcagua, Instituto de Investigaciones Geológicas, Santiago, Chile, 70 pp., 1960.
- Allmendinger, R.W., Cardozo, N., and Fisher, D.M.: *Structural Geology Algorithms: Vectors and Tensors*, Cambridge University Press, New York, United States of America, 2012.
- Alvarado, P., Barrientos, S., Sáez, M., Astroza, M., and Beck, S.: Source study and tectonic implications of the historic 1958 Las Melosas crustal earthquake, Chile, compared to earthquake damage, *Physics of the Earth and Planetary Interiors*, 175 (1-2), 26-36, 2019.
- Aron, F., Allmendinger, R.W., Cembrano, J., González, G., and Yáñez, G.: Permanent fore-arc extension and seismic segmentation: Insights from the 2010 Maule earthquake, Chile, *Journal of Geophysical Research: Solid Earth*, 118, 1-16, doi: 10.1029/2012JB009339, 2013.
- [Bird, P., and Piper, K.: Plane-stress finite-element models of tectonic flow in southern California, \*Physics of the Earth and Planetary Interiors\*, 21, 158-175, 1980.](https://doi.org/10.1029/1979JB01318)
- Cembrano, J. and Lara, L.: The link between volcanism and tectonics in the southern volcanic zone of the Chilean Andes: A review, *Tectonophysics*, 471, 96-113, doi: 10.1016/j.tecto.2009.02.038, 2009.
- Charrier, R., Baeza, O., Elgueta, S., Flynn, J. J., Gans, P., Kay, S. M., Munoz, N., Wyss, A. R., and Zurita, E.: Evidence for Cenozoic extensional basin development and tectonic inversion south of the flat-slab segment, southern Central Andes, Chile (33° -36° SL), *Journal of South American Earth Sciences*, 15 (1), 117-139, 2002.
- Chernicoff, C.J., Richards, J.P., Zappettini, E.O.: Crustal lineament control on magmatism and mineralization in northwestern Argentina: geological, geophysical, and remote sensing evidence, *Ore Geology Reviews*, 21, 127-155, 2002.
- Creixell, C., Parada, M.A., Morata, D., Vásquez, P., Pérez de Arce, C., and Arriagada, C.: Middle-Late Jurassic to Early Cretaceous transtension and transpression during arc building in Central Chile: evidence from mafic dike swarms, *Andean Geology*, 38, 37-63, 2011.
- [Deckart, K., Clark, A.H., Cuadra, P., and Fanning, M.: Refinement of the time-space evolution of the giant Mio-Pliocene Rio Blanco-Los Bronces porphyry Cu-Mo cluster, Central Chile: new U-Pb \(SHRIMP II\) and Re-Os geochronology and Ar-40/Ar-39 thermochronology data, \*Mineralium Deposita\*, 48, 57-79, 2013.](https://doi.org/10.1017/j.erd.2013.11)

- 455 [Deckart, K., Silva, W., Spröhnle, C. and Vela, I.: Timing and duration of hydrothermal activity at the Los Bronces porphyry cluster: an update, \*Mineralium Deposita\*, 49, 535-546, doi: 10.1007/s00126-014-0512-9, 2014.](#)
- Del Valle, F., Marquardt, C., Valdivia, D., Elgueta, S., and Yáñez, G.: Tasa de alzamiento neotectónico del margen costero entre Los Vilos y Santo Domingo, in: *Proceedings of the 15th Chilean Geological Congress*, Concepción, Chile, 18-23 November 2018, 1305-1307, 2018.
- 460 [England, P., and McKenzie, D.: A thin viscous sheet model for continental deformation, \*Geophysical Journal of the Royal Astronomical Society\*, 70, 295-321, 1982.](#)
- [England P., Houseman, G., and Sonder, L.: Length scales for continental deformation in convergent, divergent, and strike-slip environments: analytical and approximate solutions for thin viscous sheet models, \*Journal of Geophysical Research\*, 95, B5, 3551-3557, 1985.](#)
- 465 [Famin, V., Raimbourg, H., García, S., Bellahsen, N., Hamada, Y., Boullier, A.M., Fabbri, O., Michon, L., Uchide, T., Ricci, T., Hirono, T., and Kawabata, K.: Stress rotations and the long-term weakness of the Median Tectonic Line and the Rokko-Awaji Segment, \*Tectonics\*, 33, 1900–1919, doi: 10.1002/2014TC003600, 2014.](#)
- [Farías, M., Comte, D., Charrier, R., Martinod, J., David, C., Tassara, A., Tapia, F., and Fock, A.: Crustal-scale structural architecture in central Chile based on seismicity and surface geology: Implications for Andean mountain building, \*Tectonics\*, 29, TC3006, 22 pp., doi: 10.1029/2009TC002480, 2010.](#)
- 470 Farías, M., Comte, D., Roecker, S., Carrizo, D., and Pardo, M.: Crustal extensional faulting triggered by the 2010 Chilean earthquake: The Pichilemu Seismic Sequence, *Tectonics*, 30, doi:10.1029/2011TC002888, 2011.
- [Febbo, G.E., Kennedy, L.A., Nelson, J.L., Savell, M.J., Campbell, M.E., Creaser, R.A., Friedman, R.M., van Straaten, B.I., and Stain, H.J.: The Evolution and Structural Modification of the Supergiant Mitchell Au-Cu Porphyry, Northwestern British Columbia, \*Economic Geology\*, 114 \(2\), 303-324, 2019.](#)
- 475 Fock, A.: Cronología y tectónica de la exhumación en el Neógeno de los Andes de Chile Central entre los 33° y los 34°, undergraduate thesis, Departamento de Geología, Universidad de Chile, Chile, 179 pp., 2005.
- [Fock, A., Charrier, R., Farias, M., Makshev, V., Fanning, M., and Alvarez, P.P.: Deformation and uplift of the western main Cordillera between 33° and 34°S, in: \*Proceedings of the International Symposium on Andean Geodynamics \(ISAG\)\*, Barcelona, Spain, 12-14 September 2005, 273-276, 2005.](#)
- 480 [Fox, N., Cooke, D.R., Harris, A.C., Collett, D., and Eastwood, G.: Porphyry Au-Cu mineralization controlled by reactivation of an arc-transverse volcanosedimentary subbasin, \*Geology\*, 43 \(9\), 811-814, 2015.](#)
- Fuentes, F., Aguirre, L., Vergara, M., Valdebenito, L., and Fonseca, E.: Miocene fossil hydrothermal system associated with a volcanic complex in the Andes of central Chile, *Journal of Volcanology and Geothermal Research*, 138, 139-161, 2004.
- Godoy, E.: Geología del área entre los ríos Claro del Maipo y Cachapoal, CODELCO Chile-SERNAGEOMIN, Santiago, Chile, 68 pp., 1993.
- 485 [Gow, P.A., and Walshe, J.L.: The Role of Preexisting Geologic Architecture in the Formation of Giant Porphyry-Related Cu ± Au Deposits: Examples from New Guinea and Chile, \*Economic Geology\*, 100, 819-833, 2005.](#)

- Giambiagi, L., Ramos, V.A., Godoy, E., Alvarez, P.P., and Orts, S.: Cenozoic deformation and tectonic style of the Andes, between 33° and 34° south latitude, *Tectonics*, 22, 1041, 18 pp., doi: 10.1029/2001TC001354, 2003.
- 490 Hardebeck, J.L., and Michael, A.J.: Stress orientations at intermediate angles to the San Andreas Fault, California, *Journal of Geophysical Research*, 109, B11303, doi: 10.1029/2004JB003239, 2004.
- Harrington, R.: The Diamante Caldera and Maipo Caldera Complex in the southern Andes of Argentina and Chile (34°10' South), *Revista de la Asociación Geológica Argentina*, 44 (1-4), 186-193, 1989.
- Hernández, L.: Rocas máficas y ultramáficas en Laguna Verde, Chile central, undergraduate thesis, Departamento de Geología, Universidad de Chile, Chile, 170 pp., 2006.
- 495 Hicks, S.P., and Rietbrock, A.: Seismic slip on an upper-plate normal fault during a large subduction megathrust rupture, *Nature Geoscience*, 8, 955-961, doi: 10.1038/NGEO2585, 2015.
- Hua, Y., Zhao, D., Xu, Y., and Wang, Z.: Arc-arc collision caused the 2018 Eastern Iburi earthquake (M 6.7) in Hokkaido, Japan, *Scientific Reports* 9, 13914, doi: 10.1038/s41598-019-50305-x, 2019.
- 500 Jackson, S.E., Pearson, N.J., Griffin, W.L., and Belousova, E.A.: The application of laser ablation-inductively coupled plasma-mass spectrometry to in situ U-Pb zircon geochronology, *Chemical Geology*, 211, 47–69, 2004.
- Kay, S.M., Godoy, E., and Kurtz, A.: Episodic arc migration, crustal thickening, subduction erosion, and magmatism in the south-central Andes, *Geological Society of America Bulletin*, 117, 67–88, doi: 10.1130/B25431.1, 2005.
- Klohn, C.: Geología de la Cordillera de los Andes de Chile Central, Instituto de Investigaciones Geológicas, Santiago, Chile, 95 pp., 1960.
- 505 Kuna, V.M., Nábeček, J.L., Braunmiller, J.: Mode of slip and crust-mantle interaction at oceanic transform faults, *Nature Geoscience*, 12, 138–142, 2019.
- Kurtz, A.C., Kay, S.M., Charrier, R., and Farrar, E.: Geochronology of Miocene plutons and exhumation history of the El Teniente region, Central Chile (34-35°S), *Revista Geológica de Chile*, 24, 75-90, 1997.
- 510 Lanza, F., Tibaldi, A., Bonali, F.L., and Corazzato, C.: Space–time variations of stresses in the Miocene–Quaternary along the Calama–Olacapato–El Toro Fault Zone, Central Andes, *Tectonophysics*, 593, 33-56, 2013.
- Lavenu, A. and Cembrano, J.: Quaternary compressional deformation in the Main Cordillera of Central Chile (Cajón del Maipo, east of Santiago), *Revista Geológica de Chile*, 35, 233-252, doi: 10.5027/andgeoV35n2-a03, 2008.
- Leal, D.: Caracterización y origen del Sistema de vetas de San Pedro de Nolasco, Cordillera Principal de la Región Metropolitana, Chile central, undergraduate thesis, Instituto de Ciencias de la Tierra, Universidad Austral de Chile, Chile, 124 pp., 2019.
- 515 Maksaev, V., Munizaga, F., McWilliams, M., Fanning, M., Mathur, R., Ruiz, J., and Zentilli, M.: New Chronology for El Teniente, Chilean Andes, from U/Pb, <sup>40</sup>Ar/<sup>39</sup>Ar, Re/Os and fission-track dating: Implications for the evolution of a supergiant porphyry Cu-Mo deposit, *Society of Economic Geologists Special Publication*, 11, 15-54, 2004.
- 520 Maksaev, V., Townley, B., Palacios, C., and Camus, F.: Metallic ore deposits, in: *Geology of Chile*, edited by: Moreno, T. and Gibbons, W., The Geological Society, London, United Kingdom, 179-199, 2007.

- McCuaig, T.C. and Hronsky, J.M.A.: The mineral system concept: the key to exploration targeting, Society of Economic Geologists Special Publication, 18, 153–176, 2014.
- Mpodozis, C. and Cornejo, P.: Cenozoic tectonics and porphyry copper systems of the Chilean Andes, Society of Economic Geologists Special Publication, 16, 329-360, 2012.
- Nealy, J.L., Herman, M.W., Moore, G.L., Hayes, G.P., Benz, H.M., Bergman, E.A., and Barrientos, S.E.: 2017 Valparaíso earthquake sequence and the megathrust patchwork of central Chile, *Geophysical Research Letters*, 44, 8865–8872, doi: 10.1002/2017GL074767, 2017.
- Pardo-Casas, F., and Molnar, P.: Relative motion of the Nazca (Farallon) and South American plates since Late Cretaceous times, *Tectonics*, 6 (3), 233-248, 1987.
- Petit, J.P.: Criteria for the sense of movement on fault surfaces in brittle rocks, *Journal of Structural Geology*, 9 (5/6), 597-608, 1987.
- Piquer, J.: Structural Geology of the Andes of Central Chile: Controls on Magmatism and the Emplacement of Giant Ore Deposits, Ph. D. thesis, CODES, University of Tasmania, Australia, 200 pp., 2015.
- Piquer, J., Skarmeta, J., and Cooke, D.R.: Structural evolution of the Rio Blanco-Los Bronces district, Andes of central Chile: controls on stratigraphy, magmatism and mineralization, *Economic Geology*, 110, 1995-2023, doi: 10.2113/econgeo.110.8.1995, 2015.
- Piquer, J., Berry, R.F., Scott, R.J., and Cooke, D.R.: Arc-oblique fault systems: their role in the Cenozoic structural evolution and metallogenesis of the Andes of central Chile, *Journal of Structural Geology*, 89, 101-117, doi: 10.1016/j.jsg.2016.05.008, 2016.
- Piquer, J., Hollings, P., Rivera, O., Cooke, D.R., Baker, M., and Testa, F.: Along-strike segmentation of the Abanico Basin, central Chile: new chronological, geochemical and structural constraints, *Lithos*, 268, 174-197, doi: 10.1016/j.lithos.2016.10.025, 2017.
- Piquer, J., Yáñez, G., Rivera, O., and Cooke, D.R.: Long-lived crustal damage zones associated with fault intersections in the high Andes of Central Chile, *Andean Geology*, 46 (2), 223-239, doi: 10.5027/andgeoV46n2-3106, 2019.
- Richards, J.P., Boyce, A.J., and Pringle, M.S.: Geologic evolution of the Escondida area, northern Chile: a model for spatial and temporal localization of porphyry Cu mineralization, *Economic Geology*, 96, 271-305, 2001.
- Richards, J.P., Jourdan, F., Creaser, R.A., Maldonado, G. and DuFrane, S.A.: Geology, geochemistry, geochronology, and economic potential of Neogene volcanic rocks in the Laguna Pedernal and Salar de Aguas Calientes segments of the Archibarca lineament, northwest Argentina, *Journal of Volcanology and Geothermal Research*, 258, 47–73, 2013.
- Rivera, O.: Marco geodinámico para los pórfidos cupríferos Mio-Pliocenos de Chile central: rol de estructuras translitosféricas y anomalías gravimétricas en la metalogénesis Andina, M. Sc. thesis, Departamento de Ciencias Geológicas, Universidad Católica del Norte, Chile, 214 pp., 2017.
- Rivera, O. and Cembrano, J.: Modelo de formación de cuencas volcano-tectónicas en zonas de transferencia oblicuas a la cadena Andina: el caso de las cuencas Oligo-Miocenas de Chile central y su relación con estructuras WNW-NW (33°00' –



34°30' LS), in: Proceedings of the 9<sup>th</sup> Chilean Geological Congress, Puerto Varas, Chile, 31 July-04 August 2000, 631-636, 2000.

Rivera, O. and Falcón, M. F.: Secuencias de relleno de cuencas volcano-tectónicas transversales Oligo-Miocenas en los alrededores del yacimiento El Teniente (33°45' - 34°30' LS), in: Proceedings of the 9<sup>th</sup> Chilean Geological Congress, Puerto Varas, Chile, 31 July-04 August 2000, 819-823, 2000.

Sabaj, R.: Identificación y caracterización de estructuras potencialmente activas en la cordillera de la costa entre los 33° y 33°45'S, undergraduate thesis, Departamento de Geología, Universidad de Chile, Chile, 92 pp., 2008.

Salfity, J.A.: Lineamientos transversales al rumbo andino en el noroeste argentino, in: Proceedings of the 4th Chilean Geological Congress, Antofagasta, Chile, 19-24 August 1985, 119-137, 1985.

Saric, N., Kreft, C., and Huete, C.: Geología del yacimiento Lo Aguirre, Chile, Revista Geológica de Chile, 30 (2), 317-331, 2003.

SERNAGEOMIN: Carta Magnética de Chile 1:250.000, Santiago sheet, Servicio Nacional de Geología y Minería, Santiago, 1 map, 1980.

SERNAGEOMIN: Mapa Geológico de Chile 1:1.000.000, Servicio Nacional de Geología y Minería, Santiago, Carta Geológica de Chile, Serie Geología Básica 75, 1 map in 3 sheets, 2002.

Spagnotto, S., Triep, E., Giambiagi, L., and Lupari, M.: Triggered seismicity in the Andean arc region via static stress variation by the MW = 8.8, February 27, 2010, Maule earthquake, Journal of South American Earth Sciences, 63, 36-47, 2015.

Stern, C.R., Amini, H., Charrier, R., Godoy, E., Hervé, F., and Varela, J.: Petrochemistry and age of rhyolitic pyroclastic flows which occur along the drainage valleys of the río Maipo and río Cachapoal (Chile) and the río Yaucha and río Papagayos (Argentina), Revista Geológica de Chile, 23, 39-52, 1984.

Thomas, H.: Informe de la comisión geológica Thomas-Junge sobre la alta cordillera entre el río Aconcagua y el río Colorado, CORFO, Santiago, Chile, 76 pp., 1953.

Townley, B., Makshev, V., Palacios, C., Hernández, T., Hurtado, R., Jorquera, R., and Gonzalez, E.: Mineralización aurífera en la Cordillera de la Costa en Chile central: distritos Antena (V Región) y Colliguay (Región Metropolitana), in Proceedings of the 9th Chilean Geological Congress, Puerto Varas, Chile, 31 July-04 August 2000, 171-175, 2000.

Weinrebe, R.W. and Hasert, M.: Bathymetric Charts of the South East Pacific with links to gridded datasets, PANGAEA, <https://doi.org/10.1594/PANGAEA.785515>, 2012.

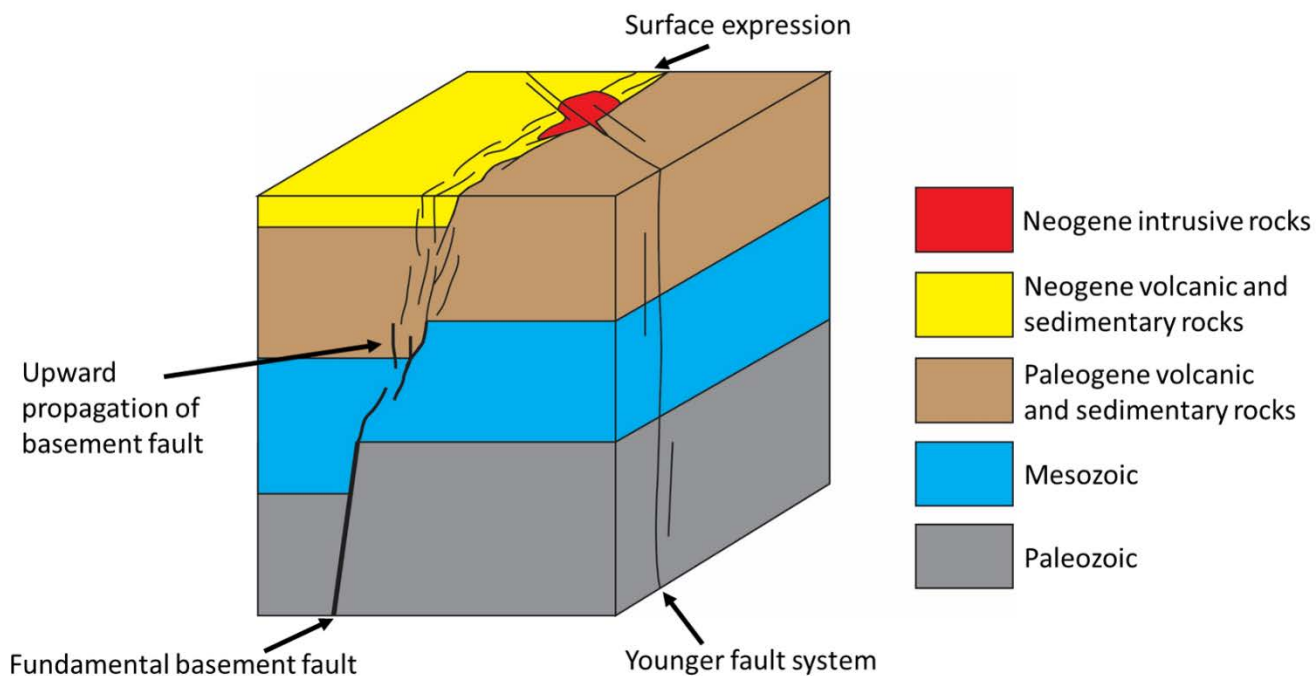
Yamaji, A.: The multiple inverse method: a new technique to separate stresses from heterogeneous fault-slip data, Journal of Structural Geology, 22, 441-452, 2000.

Yáñez, G. and Rivera, O.: Crustal dense blocks in the fore-arc and arc region of Chilean ranges and their role in the magma ascent and composition: Breaking paradigms in the Andean metallogeny, Journal of South American Earth Sciences, 93, 51-66, doi: 10.1016/j.jsames.2019.04.006, 2019.

Yáñez, G., Gana, P., and Fernández, R.: Origen y significado geológico de la Anomalía Melipilla, Chile central, Revista Geológica de Chile, 25 (2), 175-198, 1998.












590 Yáñez, G., Cembrano, J., Pardo, M., Ranero, C., and Sellés, D.: The Challenger-Juan Fernández-Maipo major tectonic transition of the Nazca-Andean subduction system at 33-34°S: geodynamic evidence and implications, *Journal of South American Earth Sciences*, 15, 23-38, 2002.

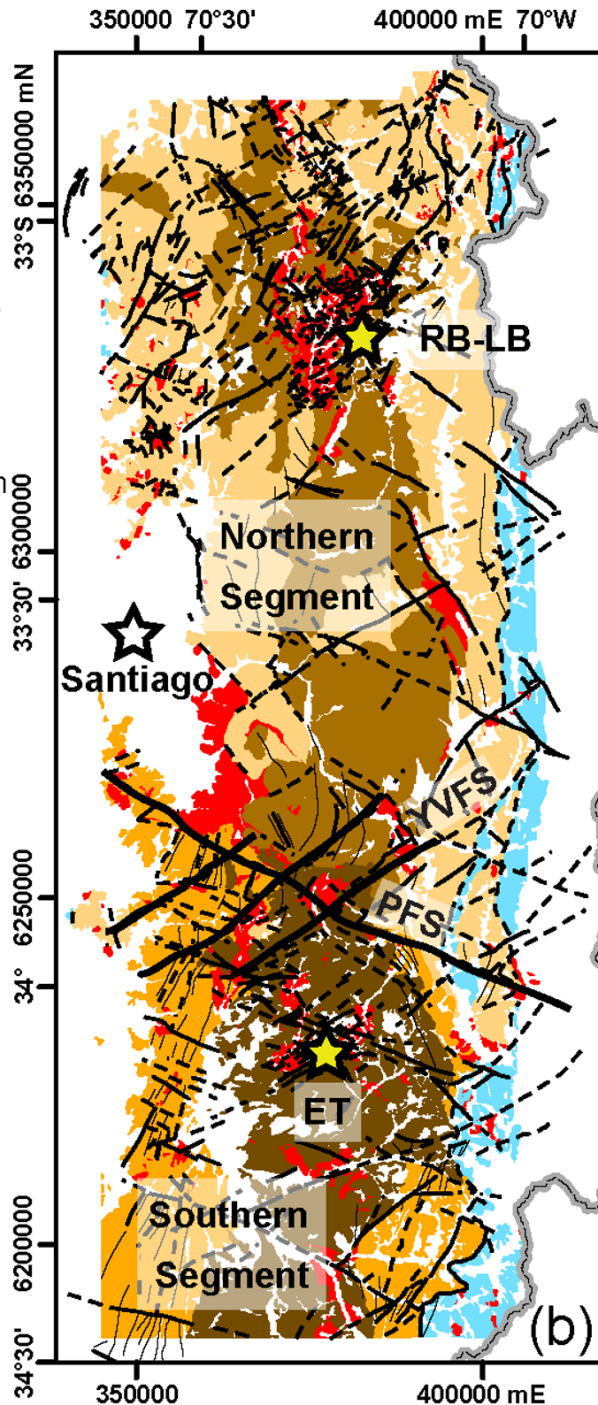
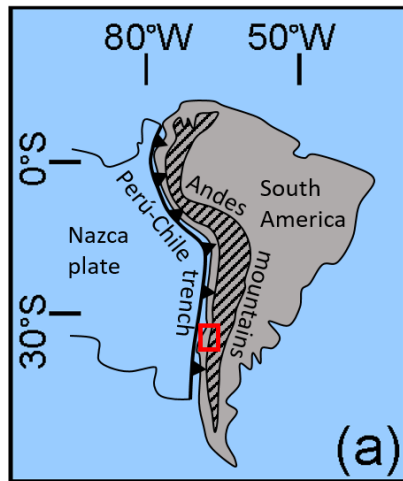
Yáñez, G., Muñoz, M., Flores-Aqueveque, V., and Bosh, A.: Gravity derived depth to basement in Santiago Basin, Chile: implications for its geological evolution, hydrogeology, low enthalpy geothermal, soil characterization and geo-hazards, 595 *Andean Geology*, 42, 147-172, doi: 10.5027/andgeoV42n2-a01, 2015.



600 **Figure 1: Schematic diagram showing how Fundamental Basement Structures (FBSs) propagate upwards through younger rocks, being represented at the current surface by a network of minor faults, often difficult to recognize in the field. The diagram also illustrates the common re-activation of this type of faults as basin-bounding faults under extensional conditions, and the relationship between fundamental basement faults and the emplacement of intrusive complexes. A younger, cross-cutting fault system is also illustrated. Adapted from Figure 7 of McCuaig and Hronsky (2014) and Figure 9 of Piquer et al. (2019).**

### Legend (map b)

-  Chile-Argentina border
-  Quaternary sediments and volcanic deposits
-  Neogene intrusive rocks
-  Teniente Volcanic Complex
-  Farellones Formation
-  Coya-Machali Formation
-  Abanico Formation
-  Mesozoic sedimentary rocks
-  Inferred fault
-  Fault
-  Fold



605

Figure 2: A. Location of the study area (red rectangle) in South America. B. Geology of the Andes of central Chile, based on Rivera and Falcón (2000), SERNAGEOMIN (2002), Fuentes et al. (2004), Fock (2005) and this work. Quaternary sediments and volcanic deposits not shown. PFS = Piuquencillo Fault System, YVFS = Yeso Valley Fault System, RB-LB = Río Blanco – Los Bronces, ET = El Teniente.

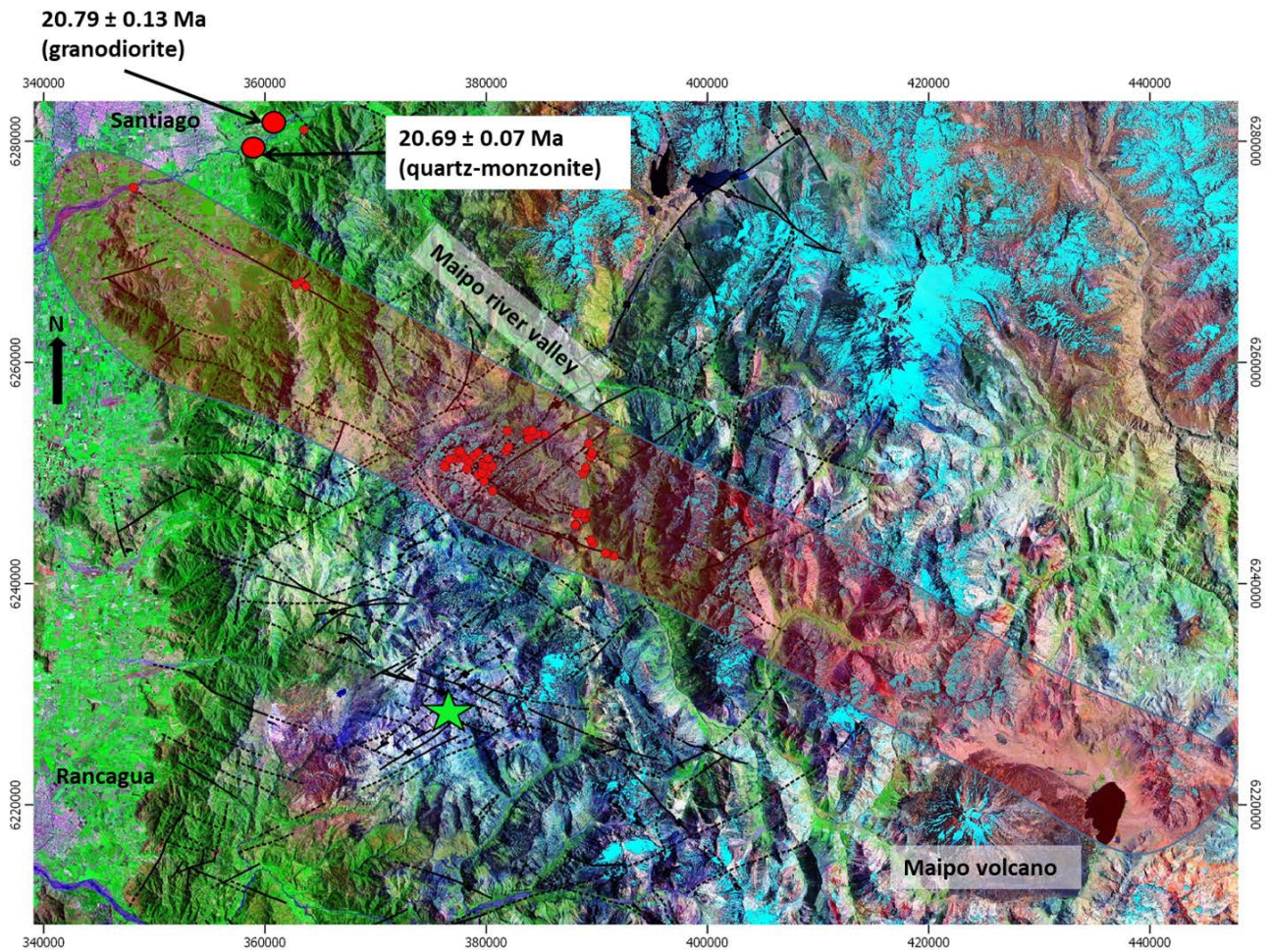
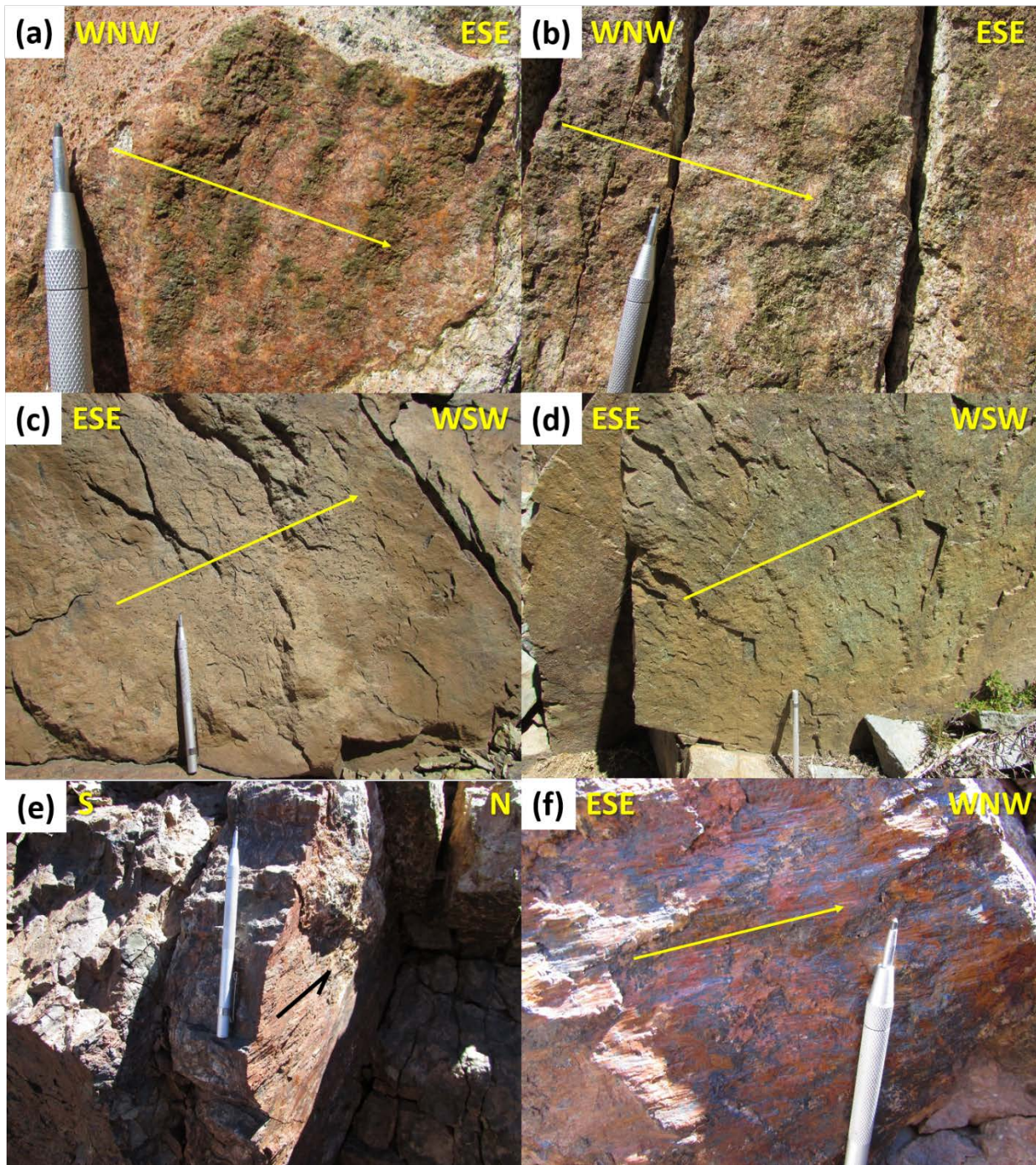


Figure 3: Distribution of structural stations (red dots) and sample location for U-Pb zircon ages. Semi-transparent red polygon shows the approximate boundary extent of the PFS; green star shows the location of the El Teniente porphyry Cu-Mo deposit. The background correspond to a Landsat image, courtesy of the U.S. Geological Survey.



615

Figure 4: Fault planes in different branches of the PFS. All of them show evidences of sinistral strike-slip movements. (a) and (b) correspond to fault planes affecting the Miocene plutons of the Carlota Intrusive Complex, with syn-tectonic epidote (a) and actinolite (b) forming steps and crystallizing in strain fringes. (c) and (d) correspond to fault planes affecting volcanic rocks of the Teniente Volcanic Complex, with sense of movement indicated by RM criteria (Petit, 1987). (e) and (f) illustrate the syn-tectonic, quartz-barite-calcite-hematite San Pedro de Nolasco veins, with the sense of movement indicated by steps in quartz and hematite.

620

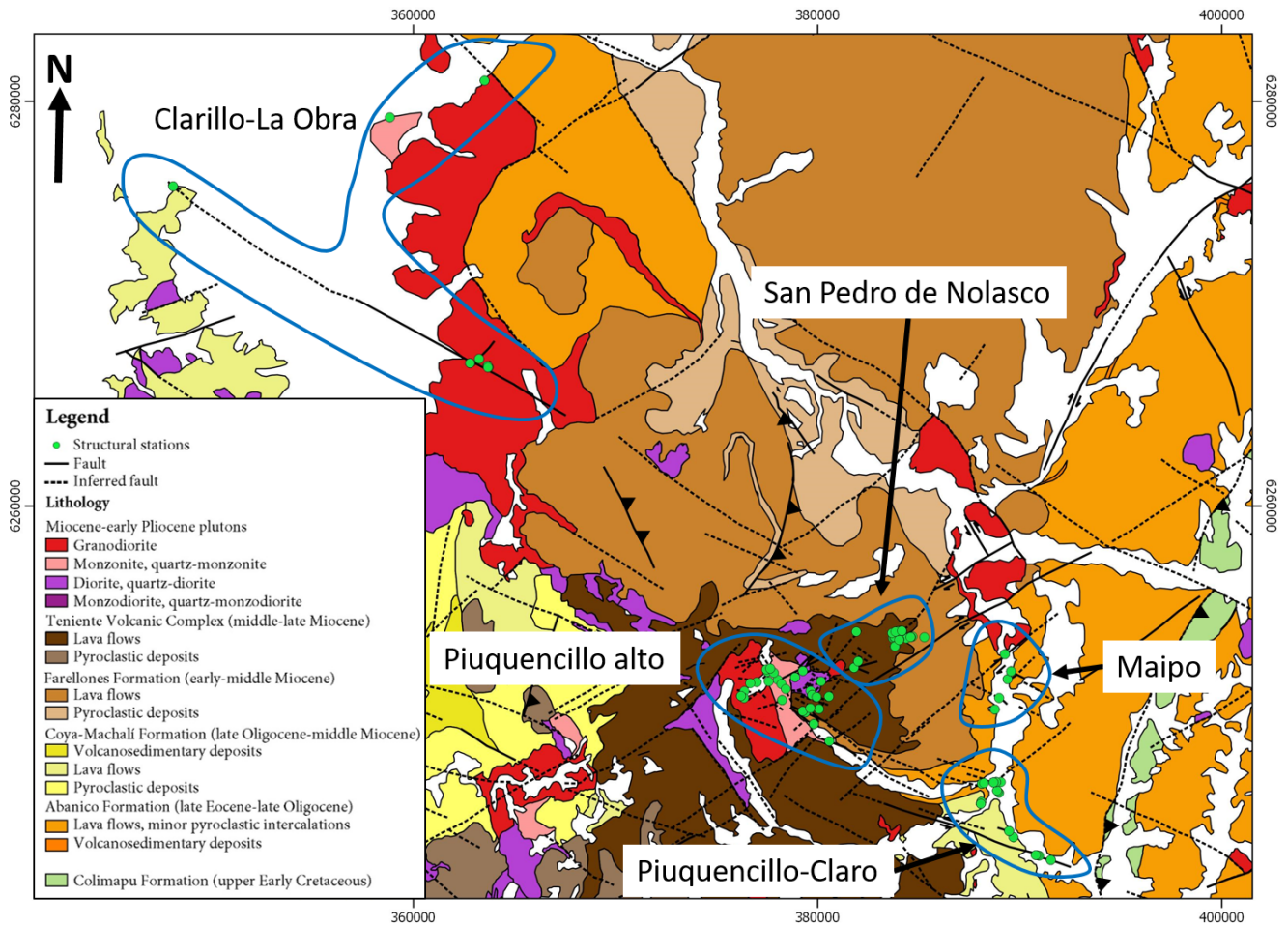


**Figure 5: Subdivision of the study area into five sectors for the analysis of preferred orientations and the calculation of strain axes and stress tensors. Geological map in the background compiled from Rivera and Cembrano (2000), SERNAGEOMIN (2002), Fock (2005), Fock et al. (2005), Piquer (2015) and this work. The background correspond to a Landsat image, courtesy of the U.S. Geological Survey.**

625

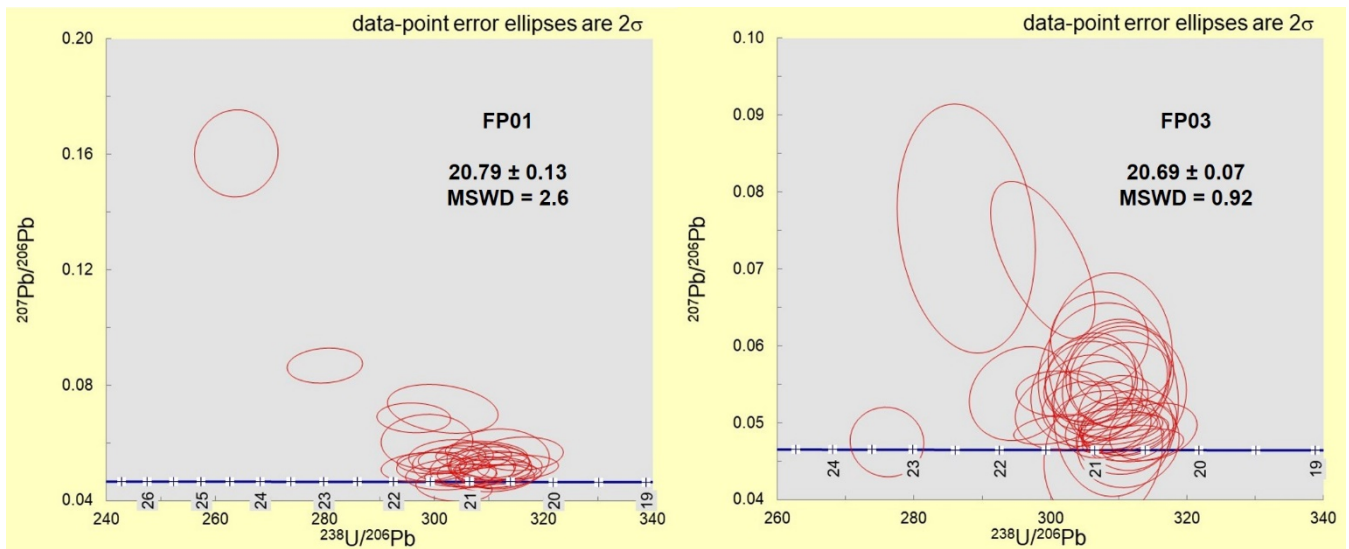


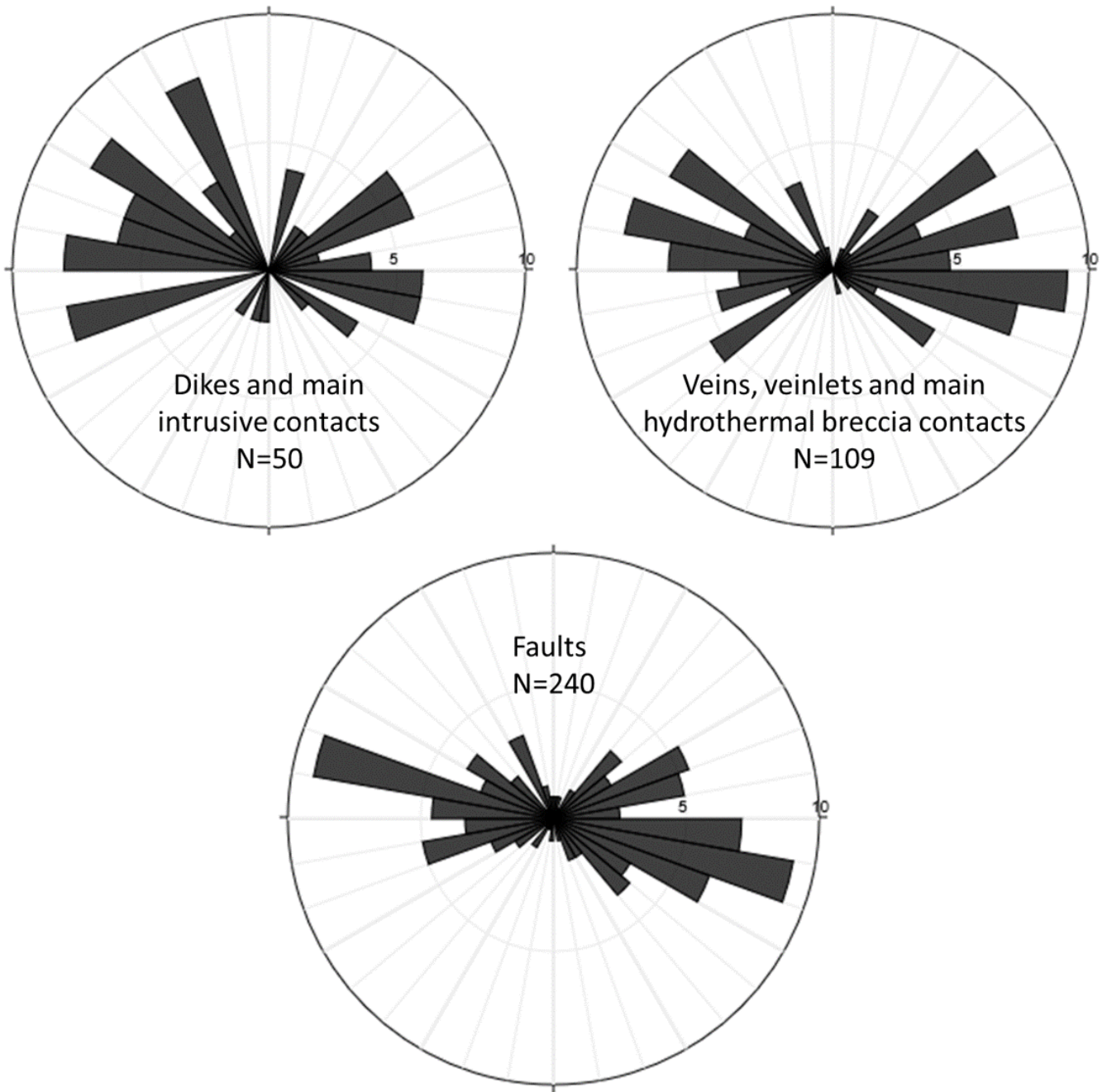
Figure 6: Tera-Wasserburg plots for the two U-Pb analyses completed for this study. Numbers on the reference concordia traces are millions of years.



Figure 7: Unconformity (dashed line) separating the flat-lying Teniente Volcanic Complex (TVC) and the gently-folded Farellones Formation. View west from the San Pedro de Nolasco vein area.

630





635 **Figure 8: Preferred orientations of dikes/main intrusive contacts, veins/main hydrothermal breccia contacts and faults, for all the study area (82 structural stations).**

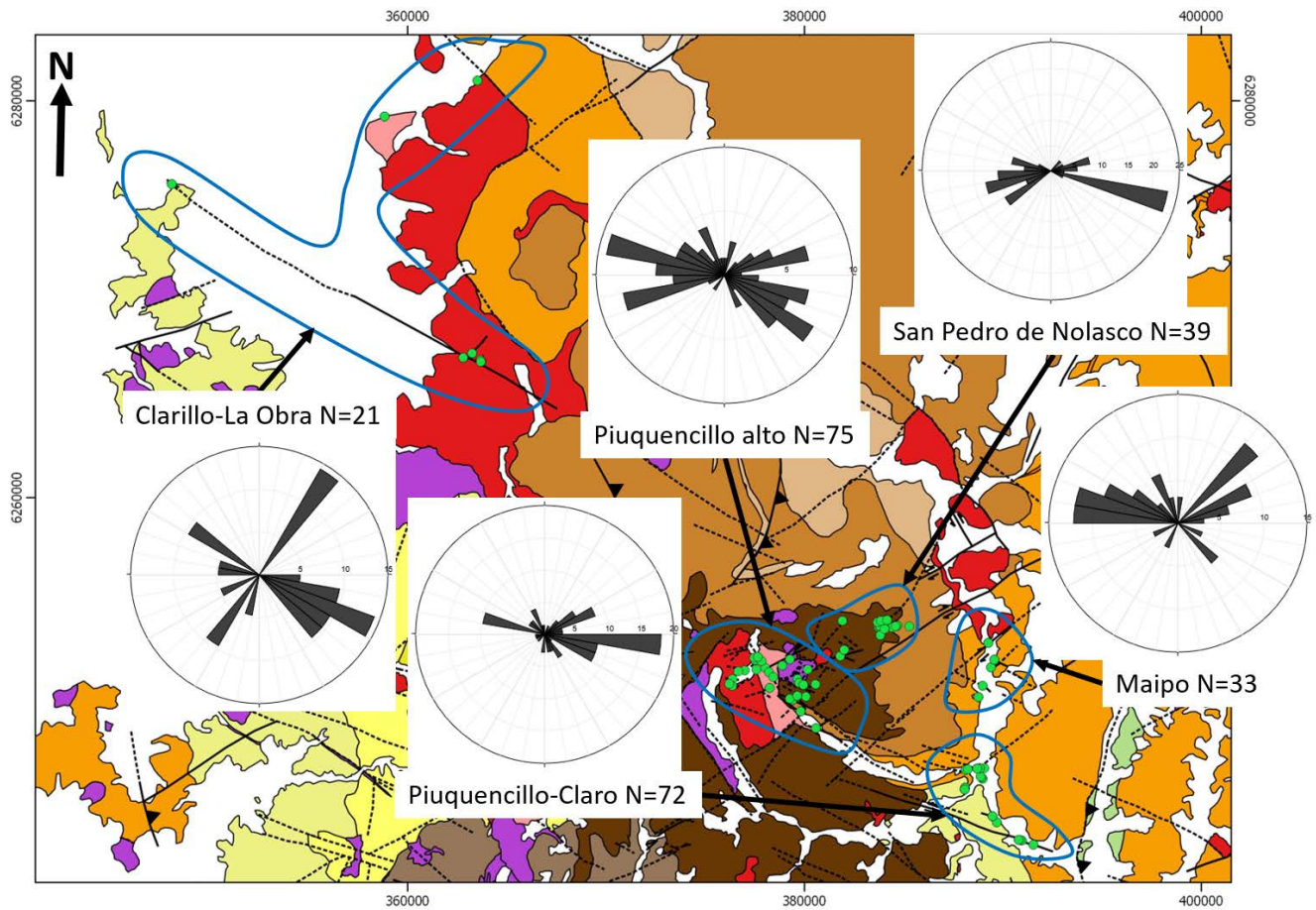
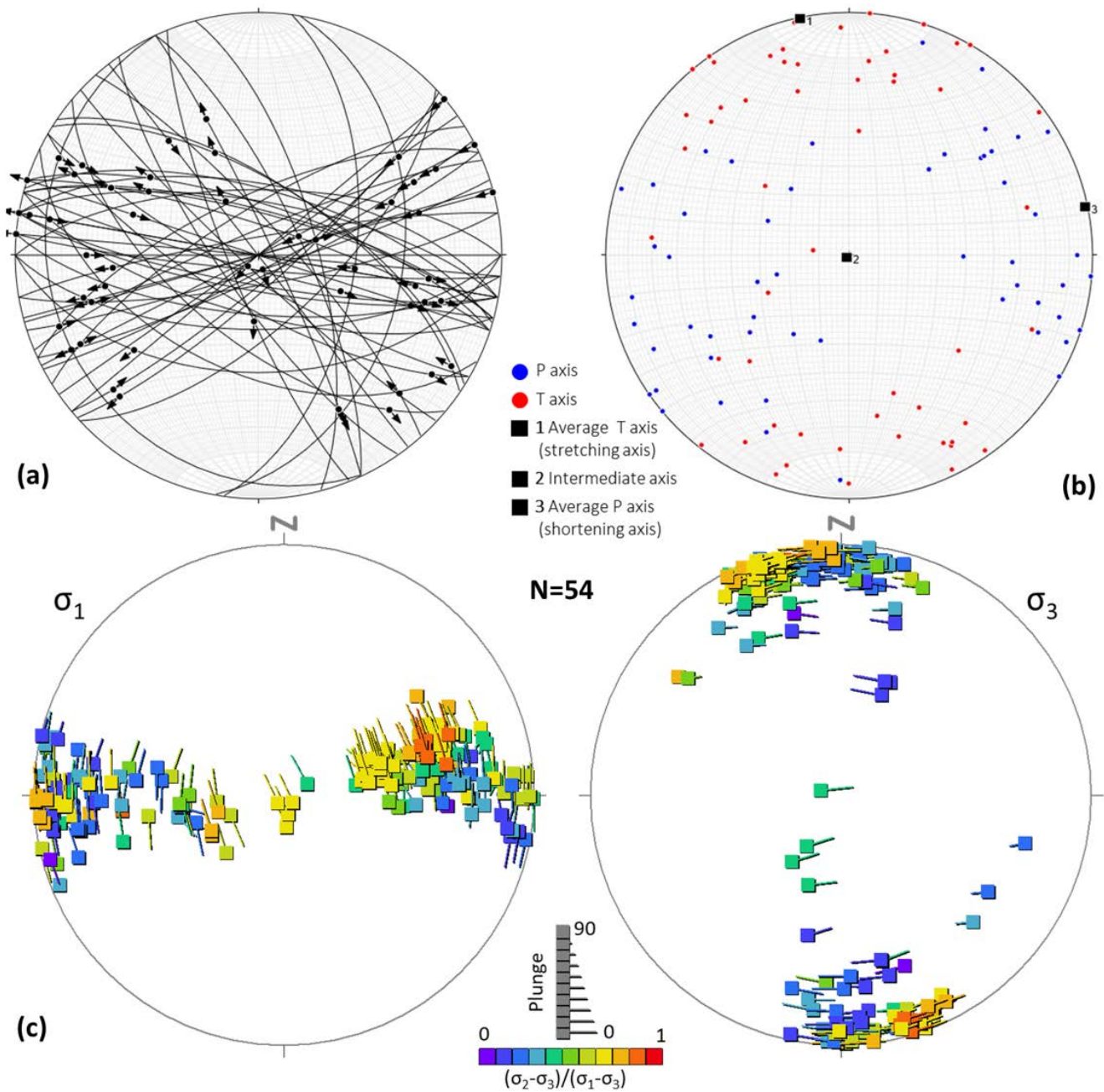
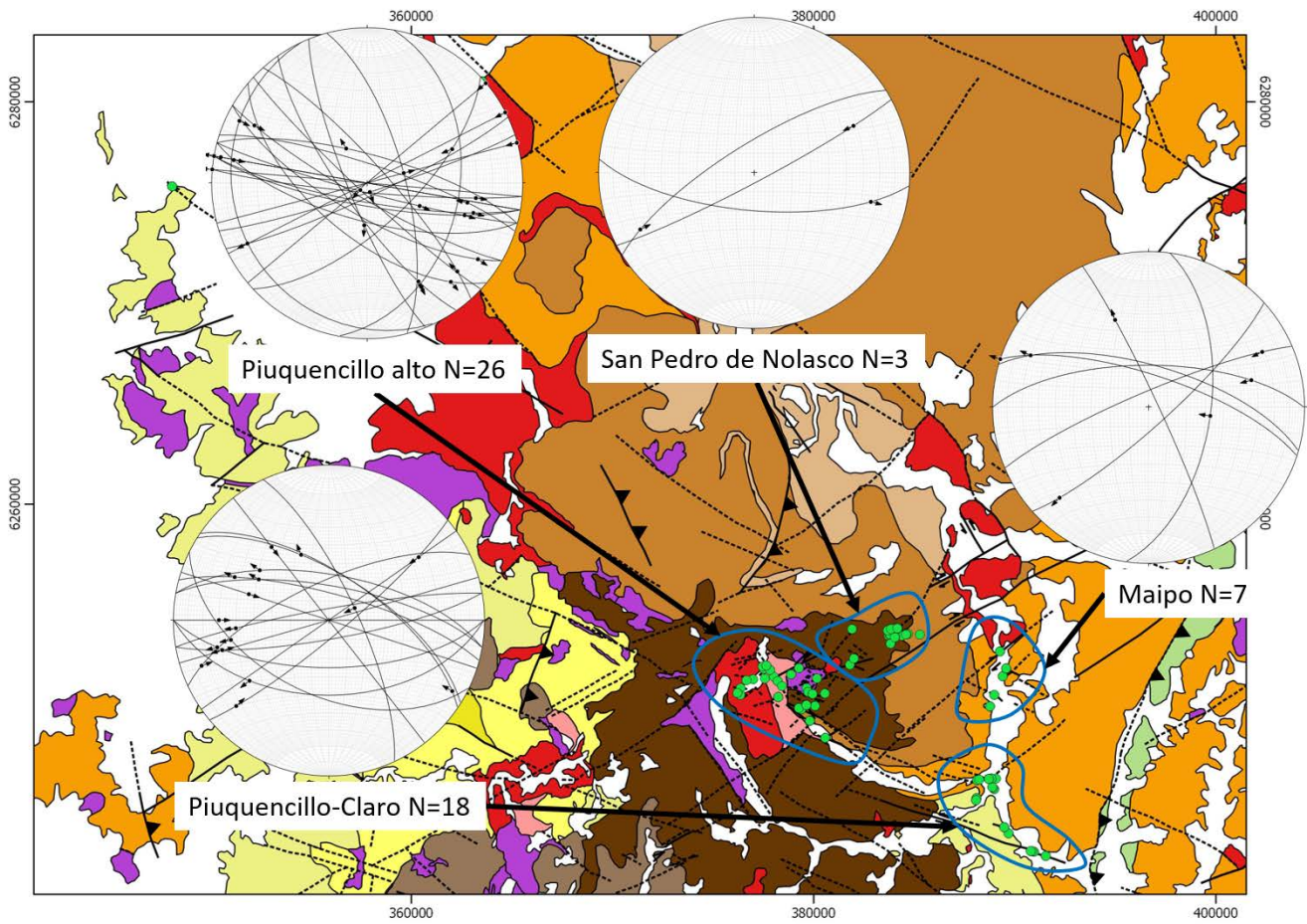


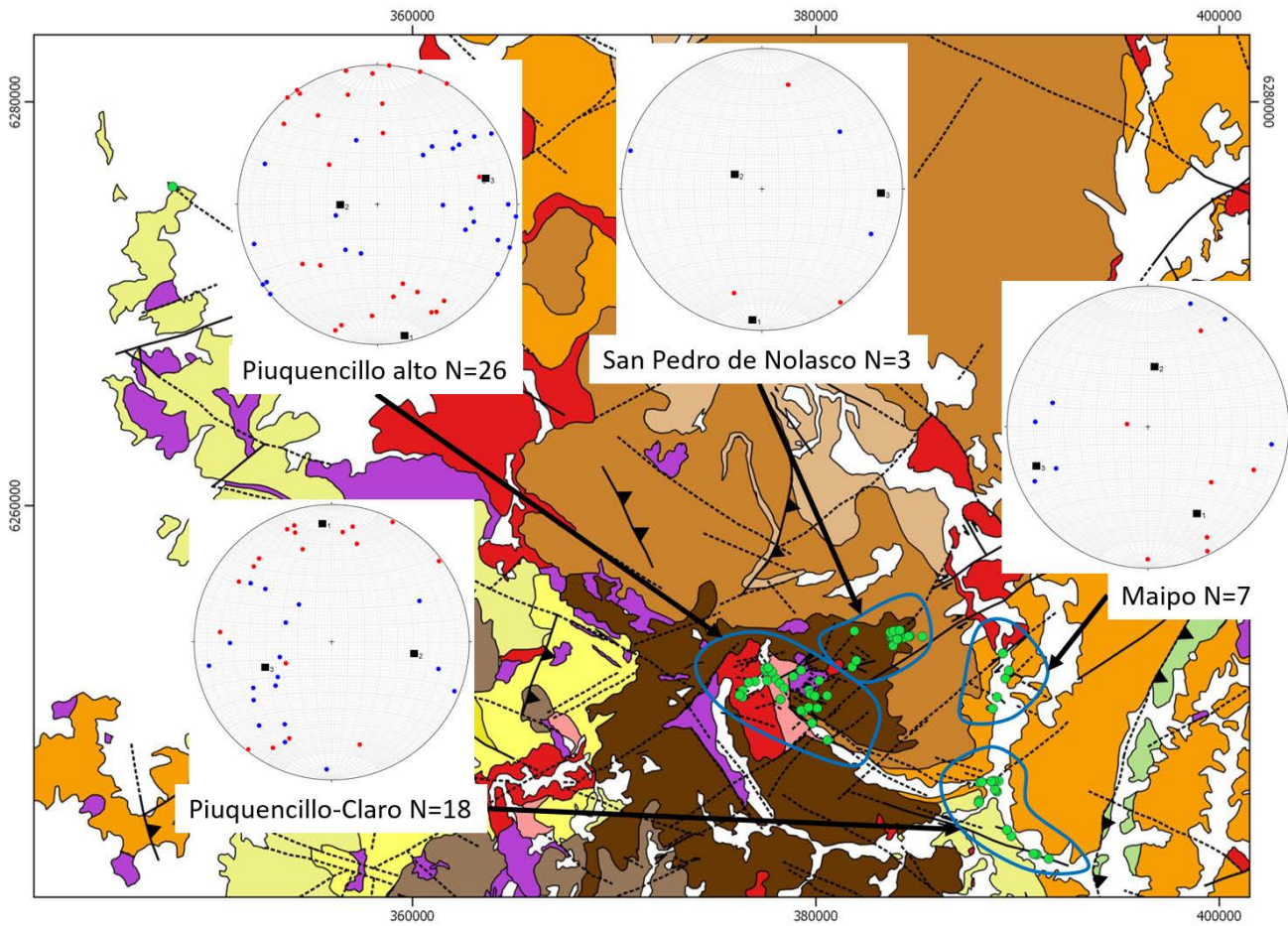
**Figure 9: Preferred orientations of fault planes in the five sectors into which the study area was subdivided. Geological map on the background as in Figure 5.**



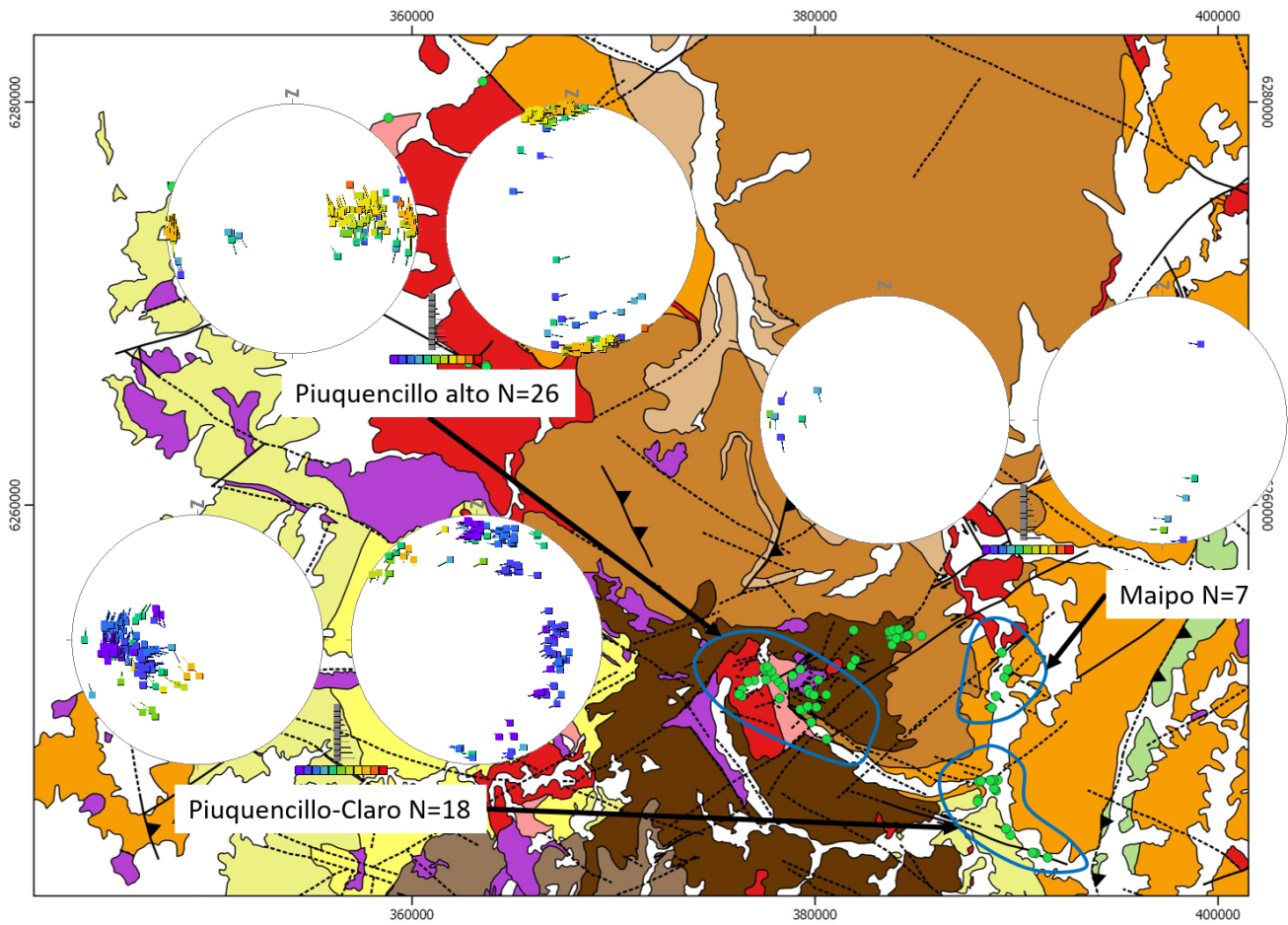
640 **Figure 10:** (a) Lower-hemisphere, equal-area projection of the 54 fault planes with kinematic information, showing also the slickenline attitudes and the sense of movement. (b) Results of the kinematic analysis for the fault planes shown in (a). P = pressure, T = tension. (c) Results of the dynamic analysis for the fault planes shown in (a). Colors represent the  $\Phi$  value calculated for each stress tensor.



645 Figure 11: Lower-hemisphere, equal-area projection of the fault planes with kinematic information by sector, showing also the slickenline attitudes and the sense of movement. **Geological map on the background as in Figure 5. The background correspond to a Landsat image, courtesy of the U.S. Geological Survey.**

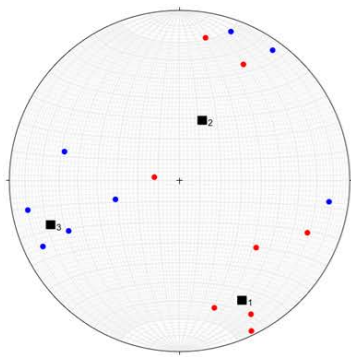


650 Figure 12: Kinematic analysis of fault plane data by sector. Clarillo-La Obra sector is not considered, as no reliable kinematic indicators were found. Geological map on the background as in Figure 5. The background correspond to a Landsat image, courtesy of the U.S. Geological Survey.

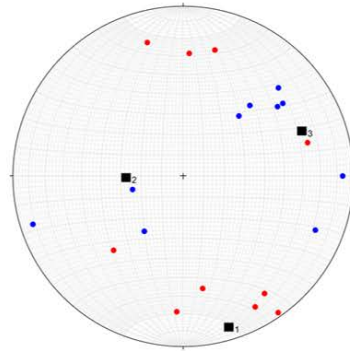


655

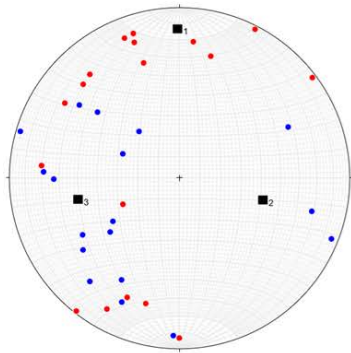
Figure 13: Dynamic analysis of fault plane data by sector. Clarillo-La Obra and San Pedro de Nolasco sectors are not considered, as the minimum of four fault planes with reliable kinematic indicators, necessary for stress state calculations, was not achieved in these areas. **Geological map on the background as in Figure 5. The background correspond to a Landsat image, courtesy of the U.S. Geological Survey.**



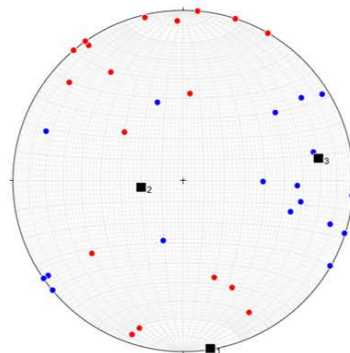
Abanico and Coya-Machalí Formations, N=8



Farellones Formation and  
Teniente Volcanic Complex, N=10

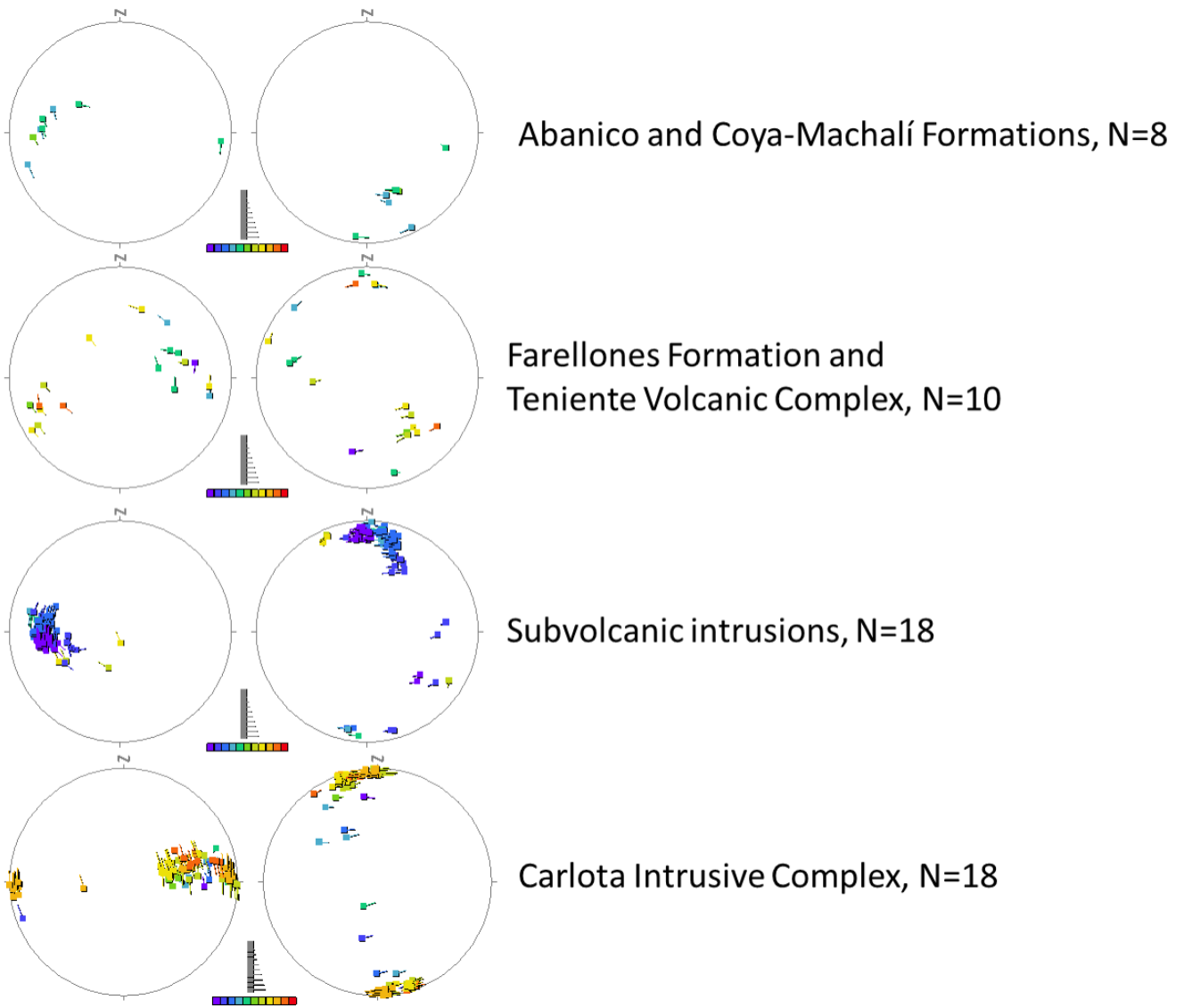


Subvolcanic intrusions, N=18



Carlota Intrusive Complex, N=18

**Figure 14: Kinematic analysis of fault plane data by lithological unit.**



660

**Figure 15: Dynamic analysis of fault plane data by lithological unit.**



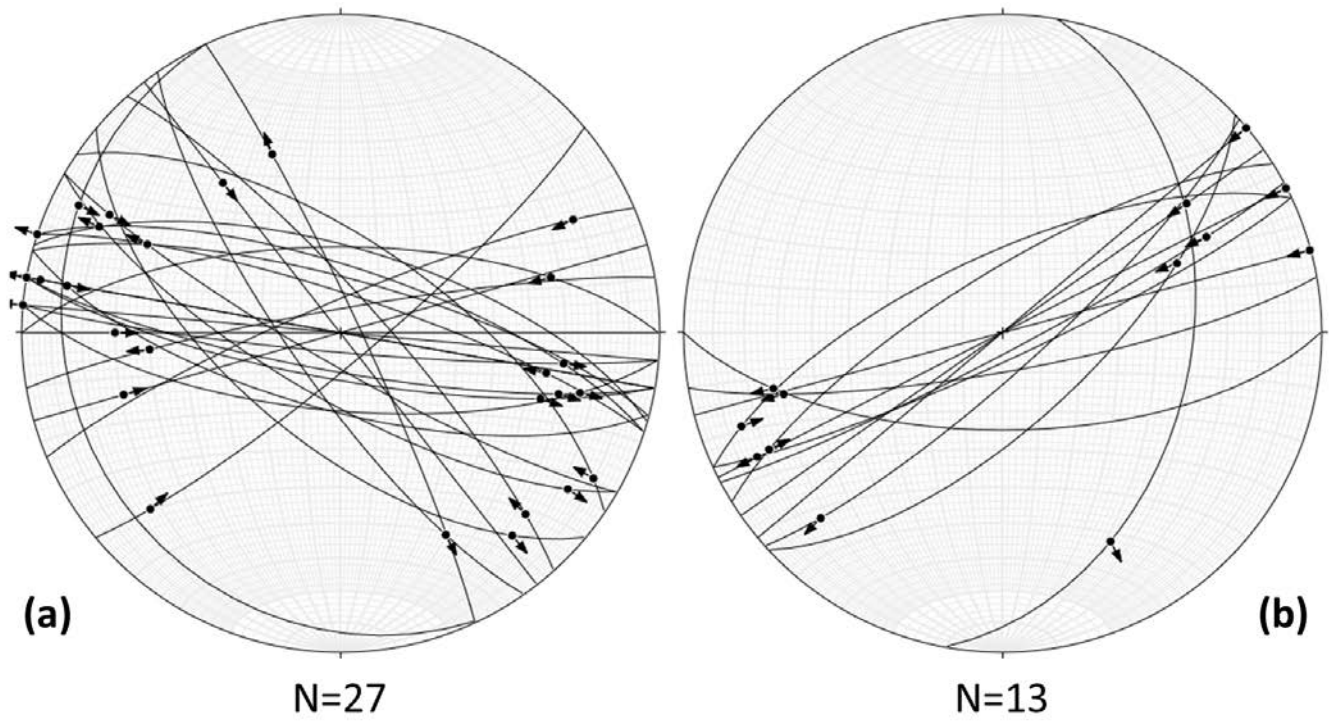
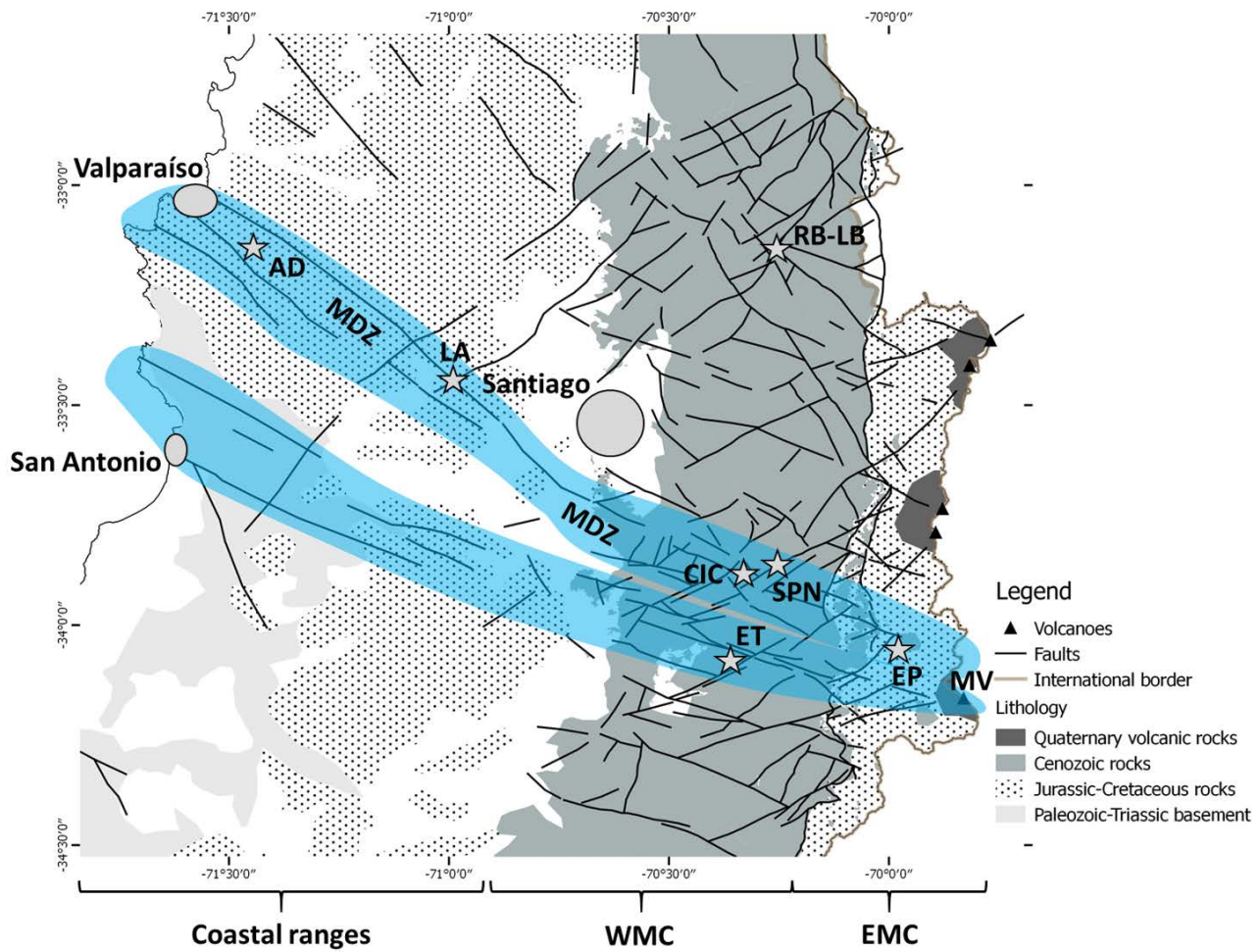


**Figure 16: (a) Lower-hemisphere, equal-area projection of fault planes with a sinistral strike-slip component and striations with pitch  $< 45^\circ$ . (b) Same as in (a) but for fault planes with a dextral slip.**



665

**Figure 16** **Figure 17:** Continental-scale expression of the Maipo deformation zone (MDZ), highlighted in light blue; the PFS correspond to its manifestation in the Cenozoic rocks of the Western Main Cordillera. Background geology from SERNAGEOMIN (2002); faults in the Western Main Cordillera from Piquer et al. (2016). RB-LB = Río Blanco-Los Bronces; ET = El Teniente; EP = Escalones prospect; SPN = San Pedro de Nolasco veins; CIC = Carlota Intrusive Complex; LA = Lo Aguirre stratabound deposit; AD = Antena District of orogenic Au veins; MV = Maipo Volcano; WMC = Western Main Cordillera; EMC = Eastern Main Cordillera. The main cities of Santiago and Valparaíso are also shown.

670

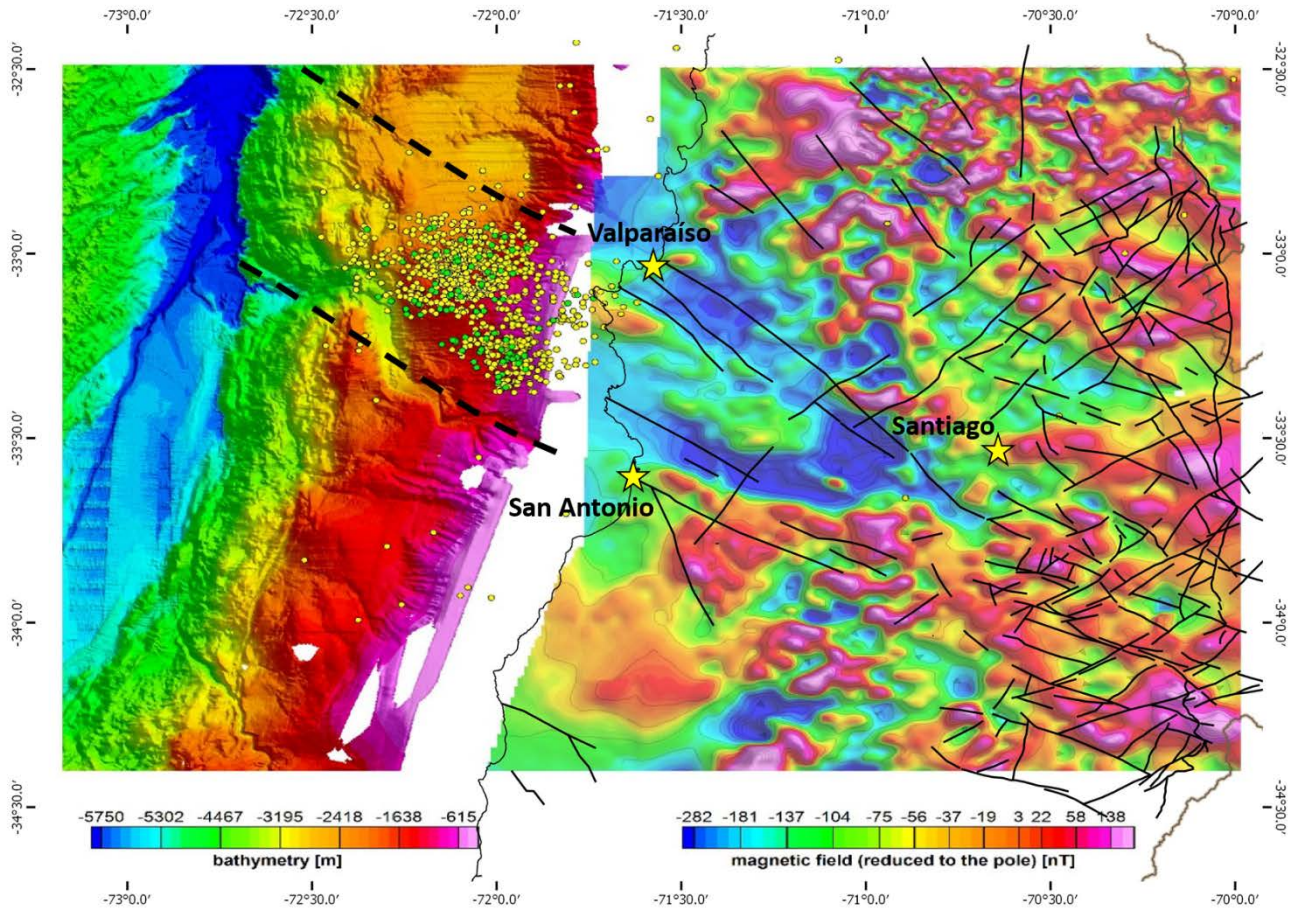


**Figure 17** **Figure 18**: Geophysical expressions of the PFS, the Maipo Deformation Zone and the Teniente-San Antonio fault system. The sub-marine continental shelf is colored according to its bathymetry (Weinrebe and Hasert, 2012); thick dashed lines represent the possible submarine prolongation of the two main branches of the MDZ. Colors in the continent correspond to RTP aeromagnetic map (SERNAGEOMIN, 1980). Yellow and green small circles show the location of earthquake hypocenters related to the 2017 Valparaíso sequence (yellow data set extracted from CSN data repository, green data set, relocated events from Nealy et al 2017, data repository). The Chile-Argentina international boundary, the coastline and fault architecture from **Fig. 16** **Fig. 17** are also shown.

680

685

Sample	N (UTM)	E (UTM)	Lithology	Age (Ma) ( $\pm 2\sigma$ )	MSWD	Number of grains
			Biotite-rich			
FP01	6281776	361704	granodiorite	20.79 $\pm$ 0.13	2.6	29
			Hornblende-rich			
FP03	6279214	358835	monzogranite	20.69 $\pm$ 0.07	0.92	34

**Table 1: Summary of U-Pb zircon geochronology of the La Obra batholith.**

### **Appendix A: U-Pb geochronology analytical procedures**

690 All the procedures described here were completed at the Geochronology Laboratory of SERNAGEOMIN (National Survey of  
 Geology and Mining, Chile) at Santiago, Chile. First the samples were sieved and crushed using standard procedures to obtain  
 a non-magnetic heavy mineral concentrate, from which zircon crystals were separated. The selected crystals were mounted in  
 epoxy glue briquettes, and then studied at a Scanning Electron Microscope, with which back-scattered electron (BSE) and  
 cathodoluminescence (CL) images were obtained.

695 At sample FP01, the selected zircon crystals vary in size between 100 and 300  $\mu\text{m}$  approximately. They correspond to igneous  
 zircons with oscillatory zoning, some of them showing evidences of inherited cores. No overgrowth was observed at crystal  
 rims. The grains contain abundant inclusions and fractures, which required a careful selection of the laser ablation spots.

At sample FP03, the selected zircon crystals vary in size between 100 and 500  $\mu\text{m}$  approximately. They correspond to igneous  
 zircons with oscillatory zoning, without observed evidences of inherited cores. Overgrowth was observed at the rims of some  
 700 crystals, and some of them display irregular borders, maybe as a result of hydrothermal processes. The grains contain very few  
 inclusions and fractures.

After spot selection based on CL and BSE images, the analyses were completed using a Thermo Fischer ElementXR ICP-MS,  
 coupled with a Photon-Machines Analyte G2 193 nm excimer laser, with a wavelength of 193 nm. U, Th and Pb concentrations  
 were calculated in relation to the reference zircon GJ-1 (Jackson et al., 2004). Isotope ratios were normalized to the same  
 705 reference zircon.

710

## Appendix B: U-Pb geochronology analytical data

Values in bold correspond to those used for age calculations.

(1) Values not considered in the calculations due to an incorrect pattern in isotopic ratio curves (isotopic content inhomogeneity)

715

<b><math>^{206}\text{Pb}/^{238}\text{U}</math> (corr by common Pb)</b>		<b><math>^{206}\text{Pb}/^{238}\text{U}</math></b>		<b><math>^{207}\text{Pb}/^{235}\text{U}</math></b>		<b><math>^{207}\text{Pb}/^{206}\text{Pb}</math></b>			<b><math>^{207}\text{Pb}/^{206}\text{Pb}</math></b>
<b>age</b>	<b>2<math>\sigma</math></b>	<b>ratio</b>	<b>2<math>\sigma</math></b>	<b>ratio</b>	<b>2<math>\sigma</math></b>	<b>Rho</b>	<b>ratio</b>	<b>2<math>\sigma</math></b>	<b>Common</b>
<b>FP01</b>									
<b>21.2</b>	<b>0.5</b>	0.00330	0.00007	0.02233	0.00200	0.07485	0.04940	0.00450	0.83698
<b>20.8</b>	<b>0.5</b>	0.00326	0.00007	0.02291	0.00240	0.07219	0.05170	0.00520	0.83696
<b>21.1</b>	<b>0.5</b>	0.00335	0.00008	0.02791	0.00360	0.15235	0.06120	0.00730	0.83700
<b>21.0</b>	<b>0.4</b>	0.00330	0.00006	0.02483	0.00160	0.02329	0.05440	0.00340	0.83698
<b>21.0</b>	<b>0.4</b>	0.00328	0.00006	0.02204	0.00140	0.11814	0.04890	0.00300	0.83697
<b>20.6</b>	<b>0.4</b>	0.00322	0.00006	0.02310	0.00280	0.18976	0.05240	0.00600	0.83695
<b>20.6</b>	<b>0.4</b>	0.00323	0.00006	0.02339	0.00220	0.05477	0.05340	0.00490	0.83695
<b>20.4</b>	<b>0.5</b>	0.00321	0.00008	0.02406	0.00380	0.11754	0.05690	0.00820	0.83694
<b>21.1</b>	<b>0.4</b>	0.00338	0.00006	0.03196	0.00210	0.35555	0.06820	0.00410	0.83701
<b>21.2</b>	<b>0.4</b>	0.00329	0.00006	0.02031	0.00200	0.36009	0.04520	0.00410	0.83698
<b>21.3</b>	<b>0.4</b>	0.00334	0.00006	0.02435	0.00150	0.35256	0.05280	0.00270	0.83699
<b>20.6</b>	<b>0.4</b>	0.00321	0.00006	0.02243	0.00140	0.34455	0.05060	0.00280	0.83694
<b>20.9</b>	<b>0.6</b>	0.00379	0.00009	0.08384	0.00670	0.27281	0.16000	0.01100	0.83718
<b>20.5</b>	<b>0.4</b>	0.00321	0.00007	0.02262	0.00200	0.08329	0.05180	0.00450	0.83694
<b>21.3</b>	<b>0.4</b>	0.00333	0.00006	0.02377	0.00190	0.10277	0.05170	0.00400	0.83699
<b>20.5</b>	<b>0.4</b>	0.00321	0.00006	0.02262	0.00150	0.25837	0.05160	0.00310	0.83694
<b>20.5</b>	<b>0.4</b>	0.00320	0.00006	0.02137	0.00140	0.00231	0.04900	0.00310	0.83694
<b>21.4</b>	<b>0.5</b>	0.00336	0.00007	0.02387	0.00190	0.08780	0.05300	0.00410	0.83700
<b>20.7</b>	<b>0.4</b>	0.00325	0.00006	0.02493	0.00170	0.20271	0.05640	0.00360	0.83696
<b>20.5</b>	<b>0.4</b>	0.00322	0.00006	0.02329	0.00170	0.13290	0.05320	0.00340	0.83694
<b>20.6</b>	<b>0.6</b>	0.00332	0.00009	0.03282	0.00350	0.48085	0.07440	0.00730	0.83698
<b>20.5</b>	<b>0.4</b>	0.00323	0.00006	0.02512	0.00170	0.47512	0.05790	0.00340	0.83695

<b>21.8</b>	<b>0.5</b>	0.00357	0.00007	0.04274	0.00250	0.23171	0.08650	0.00450	0.83709
<b>21.0</b>	<b>0.5</b>	0.00330	0.00007	0.02512	0.00220	0.14942	0.05600	0.00450	0.83698
<b>20.8</b>	<b>0.4</b>	0.00325	0.00006	0.02243	0.00190	0.04361	0.05160	0.00440	0.83696
<b>20.6</b>	<b>0.4</b>	0.00321	0.00006	0.02118	0.00170	0.07506	0.04910	0.00380	0.83694
<b>21.1</b>	<b>0.4</b>	0.00330	0.00006	0.02368	0.00240	0.21186	0.05320	0.00550	0.83698
<b>20.3</b>	<b>0.4</b>	0.00317	0.00006	0.02252	0.00150	0.14284	0.05220	0.00330	0.83692
<b>20.1</b>	<b>0.4</b>	0.00317	0.00006	0.02454	0.00210	0.14760	0.05650	0.00470	0.83692
(1)		<del>0.00387</del>	<del>0.00019</del>	<del>0.07508</del>	<del>0.02200</del>	<del>0.99260</del>	<del>0.11100</del>	<del>0.01800</del>	
(1)		<del>0.00434</del>	<del>0.00011</del>	<del>0.15304</del>	<del>0.01700</del>	<del>0.11226</del>	<del>0.25300</del>	<del>0.02700</del>	
(1)		<del>0.00378</del>	<del>0.00011</del>	<del>0.07912</del>	<del>0.00560</del>	<del>0.13594</del>	<del>0.15460</del>	<del>0.00980</del>	
(1)		<del>0.00437</del>	<del>0.00031</del>	<del>0.15016</del>	<del>0.03100</del>	<del>0.99093</del>	<del>0.21300</del>	<del>0.03000</del>	
(1)		<del>0.11283</del>	<del>0.02400</del>	<del>12.51304</del>	<del>2.80000</del>	<del>0.99880</del>	<del>0.78600</del>	<del>0.01100</del>	

<sup>206</sup>Pb/<sup>238</sup>U (corr

by common Pb)

<sup>206</sup>Pb/<sup>238</sup>U

<sup>207</sup>Pb/<sup>235</sup>U

<sup>207</sup>Pb/<sup>206</sup>Pb

<sup>207</sup>Pb/<sup>206</sup>Pb

age	2σ	ratio	2σ	ratio	2σ	Rho	ratio	2σ	Common
<b>FP03</b>									
<b>21.2</b>	<b>0.4</b>	0.00332	0.00006	0.02461	0.00120	0.37242	0.05350	0.00240	0.83699
<b>20.8</b>	<b>0.4</b>	0.00327	0.00006	0.02461	0.00160	0.14300	0.05490	0.00330	0.83697
<b>20.8</b>	<b>0.4</b>	0.00324	0.00005	0.02206	0.00140	0.01562	0.04990	0.00310	0.83695
<b>20.5</b>	<b>0.5</b>	0.00324	0.00008	0.02617	0.00400	0.11329	0.05880	0.00860	0.83695
<b>20.7</b>	<b>0.4</b>	0.00325	0.00006	0.02382	0.00180	0.11766	0.05460	0.00400	0.83696
<b>20.5</b>	<b>0.4</b>	0.00326	0.00006	0.02735	0.00230	0.21824	0.06300	0.00500	0.83696
<b>20.6</b>	<b>0.4</b>	0.00321	0.00006	0.02098	0.00210	0.09036	0.04790	0.00480	0.83694
<b>21.6</b>	<b>0.5</b>	0.00338	0.00007	0.02510	0.00230	0.05167	0.05220	0.00450	0.83701
<b>21.6</b>	<b>0.7</b>	0.00348	0.00010	0.03608	0.00660	0.31855	0.07500	0.01300	0.83705
<b>20.5</b>	<b>0.5</b>	0.00322	0.00007	0.02500	0.00250	0.12196	0.05680	0.00570	0.83695
<b>21.1</b>	<b>0.4</b>	0.00331	0.00007	0.02353	0.00190	0.08736	0.05190	0.00420	0.83698
<b>20.6</b>	<b>0.4</b>	0.00322	0.00006	0.02216	0.00230	0.23467	0.04990	0.00520	0.83694
<b>20.5</b>	<b>0.5</b>	0.00322	0.00008	0.02402	0.00310	0.16945	0.05490	0.00710	0.83694

<b>20.9</b>	<b>0.5</b>	0.00325	0.00008	0.02059	0.00340	0.00612	0.04550	0.00740	0.83696
<b>20.7</b>	<b>0.3</b>	0.00322	0.00005	0.02124	0.00058	0.06152	0.04790	0.00120	0.83694
<b>20.5</b>	<b>0.4</b>	0.00323	0.00006	0.02480	0.00230	0.11619	0.05540	0.00520	0.83695
<b>20.5</b>	<b>0.4</b>	0.00322	0.00006	0.02500	0.00150	0.16404	0.05520	0.00340	0.83694
<b>20.8</b>	<b>0.4</b>	0.00327	0.00006	0.02510	0.00220	0.07492	0.05570	0.00460	0.83697
<b>20.5</b>	<b>0.3</b>	0.00319	0.00005	0.02070	0.00073	0.09545	0.04770	0.00170	0.83693
<b>20.4</b>	<b>0.3</b>	0.00317	0.00005	0.02137	0.00130	0.03120	0.04900	0.00290	0.83693
<b>20.7</b>	<b>0.3</b>	0.00322	0.00005	0.02188	0.00071	0.09875	0.04910	0.00160	0.83695
<b>20.6</b>	<b>0.6</b>	0.00325	0.00008	0.02500	0.00360	0.11666	0.05670	0.00780	0.83696
<b>21.3</b>	<b>0.3</b>	0.00333	0.00005	0.02255	0.00068	0.12092	0.04930	0.00140	0.83699
<b>20.6</b>	<b>0.4</b>	0.00321	0.00006	0.02216	0.00150	0.02902	0.04970	0.00320	0.83694
<b>20.8</b>	<b>0.4</b>	0.00326	0.00006	0.02317	0.00092	0.15464	0.05220	0.00210	0.83696
<b>20.6</b>	<b>0.3</b>	0.00322	0.00005	0.02163	0.00074	0.01478	0.04890	0.00160	0.83694
<b>20.6</b>	<b>0.6</b>	0.00323	0.00008	0.02314	0.00420	0.07568	0.05300	0.01000	0.83695
<b>20.8</b>	<b>0.5</b>	0.00328	0.00007	0.02441	0.00260	0.06892	0.05510	0.00590	0.83697
<b>20.8</b>	<b>0.4</b>	0.00327	0.00006	0.02490	0.00200	0.18788	0.05500	0.00440	0.83697
<b>20.9</b>	<b>0.4</b>	0.00327	0.00006	0.02323	0.00150	0.25362	0.05170	0.00320	0.83697
<b>20.9</b>	<b>0.5</b>	0.00335	0.00007	0.03284	0.00430	0.70012	0.07090	0.00800	0.83700
<b>20.6</b>	<b>0.4</b>	0.00321	0.00006	0.02167	0.00140	0.07098	0.04920	0.00320	0.83694
<b>20.7</b>	<b>0.3</b>	0.00323	0.00005	0.02220	0.00077	0.43799	0.05020	0.00150	0.83695
<b>20.7</b>	<b>0.4</b>	0.00322	0.00006	0.02127	0.00170	0.16802	0.04790	0.00360	0.83694
23.3	0.4	0.00362	0.00006	0.02372	0.00190	0.23066	0.04750	0.00360	0.83711
(1)		<del>0.00352</del>	<del>0.00009</del>	<del>0.05049</del>	<del>0.00650</del>	<del>0.53069</del>	<del>0.10300</del>	<del>0.01200</del>	
(1)		<del>0.00343</del>	<del>0.00010</del>	<del>0.05000</del>	<del>0.01000</del>	<del>0.91903</del>	<del>0.09400</del>	<del>0.01400</del>	
(1)		<del>0.00262</del>	<del>0.00006</del>	<del>0.01760</del>	<del>0.00093</del>	<del>0.06173</del>	<del>0.04910</del>	<del>0.00270</del>	
(1)		<del>0.00373</del>	<del>0.00007</del>	<del>0.03157</del>	<del>0.00200</del>	<del>0.07834</del>	<del>0.06150</del>	<del>0.00390</del>	